GRAPHITIC COKE IN MICROWAVE-ASSISTED CATALYTIC PYROLYSIS TO IMPROVE PROCESS EFFICIENCY AND SOIL QUALITY

by

Emma Moreside

B.A.Sc., The University of Ottawa, 2017

A THESIS SUBMITTED IN PARTIAL FULFILLMENT OF

THE REQUIREMENTS FOR THE DEGREE OF

MASTER OF APPLIED SCIENCE

in

THE FACULTY OF GRADUATE AND POSTDOCTORAL STUDIES

(Chemical and Biological Engineering)

THE UNIVERSITY OF BRITISH COLUMBIA

(Vancouver)

March 2021

The following individuals certify that they have read, and recommend to the Faculty of Graduate and Postdoctoral Studies for acceptance, a thesis entitled:

Graphitic coke in microwave-assisted catalytic pyrolysis to improve process efficiency and soil quality

submitted by Emma Moreside in partial fulfillment of the requirements for

the degree of Master of Applied Science

in Chemical and Biological Engineering

Examining Committee:

Xiaotao Bi, Chemical and Biological Engineering, UBC
Supervisor

Anthony Lau, Chemical and Biological Engineering, UBC
Supervisory Committee Member

Loretta Li, Civil Engineering, UBC
Supervisory Committee Member

Abstract

Microwave pyrolysis is an effective method of converting wood waste into valuable biochar which can be added to agricultural soils to improve water retention, structural stability, and nutrient adsorption. When coupled with advantages of catalytic coke formation, the process is improved both by increasing the efficiency of microwave absorption and the retention of fertilizers in soil. In this exploratory study, sawdust is mixed with 30 or 150 wt% potassium phosphate (K_3PO_4) as a pyrolysis feedstock. The K_3PO_4 acts both as a reaction catalyst and as a fertilizer for soils. The K_3PO_4 was separated from the biochar post-reaction and analyzed for coke formation.

Coke produced at a higher reaction temperature (550 ^oC) was found to have a greater ratio of graphitic to oxygenated coke, up to 4.5:1, while coke produced during a longer reaction time was found to increase the total coke yield. Combining the two (more graphitic coke, greater coke yield) by producing coke at 550 °C for 50 min produced coked K_3PO_4 that has the greatest microwave absorption with a loss tangent 30 times greater than fresh K_3PO_4. This improvement is likely due to greater amount of polyaromatic C=C bonds under which the 'Maxwell-Wagner-Sillars' effect takes place, releasing energy in the form of heat.

The coke layer surrounding K_3PO_4 particles was tested in soil as a nutrient release barrier. In all cases, the coke slowed the leaching of both K^+ and PO_4^- ions, up to 10 and 18 %, respectively. The slowest release was observed with low temperature coke (350 ^oC) which likely has more oxygen functional groups which can electrostatically interact with the leaching ions. The coke produced over a longer reaction time of 50 min also showed an improvement in K and P retention, likely because of the increased fraction of coke on the K_3PO_4 surface. It is estimated that coke

produced at 350 °C for 50 min would have an even better retention in K and P as it has both advantages of a higher content of oxygen functional groups and a higher yield of coke.

This exploratory study suggests that coke has the potential to both improve microwave absorption during pyrolysis and act as a slow-release barrier for fertilizers in soil. To expand the boundaries and robustness of this study, the effects should be investigated under extended microwave power, different catalysts, and soil conditions in a larger scale experimental system.

Lay Summary

Forests cover 60% of the area in British Columbia, Canada. From this huge forest area comes a large amount of wood waste from damaged trees and harvest residues. Through a thermochemical conversion process called pyrolysis, this wood waste feedstock can be upgraded into a valuable carbon-based product, ‘biochar’, which can be used to improve the quality of agricultural soils. During pyrolysis, the feedstock is mixed with a catalyst and heated to high temperatures using a microwave. In this study, the catalyst was analyzed after the pyrolysis reaction and found to have a layer of carbon ‘coke’ deposited on its surface. Under high preparation temperatures and long reaction times, this coke layer was found to be able to improve the microwave heating efficiency during the reaction. When added to agricultural soil, this coke layer was also found to delay the release of beneficial nutrients from fertilizers, prolonging their availability to crops.

Preface

The work covered in this thesis was completed by Emma Moreside under the supervision of Dr. Xiaotao Bi. This work includes a literature review, experimental design and execution, data analysis, and thesis writing and review. This thesis represents original, individual, and unpublished work by the author.

Table of Contents

List of Tables

List of Figures

List of Abbreviations

BC	British Columbia
BET	Brunauer–Emmett–Teller
CEC	Cation Exchange Capacity
CRF	Controlled Release Fertilizer
CS-GO	Chitosan and Graphene Oxide
DI	Deionized
DTG	Derivative Thermogravimetric Analysis
EA	Elemental Analysis
ESC	European Standardization Committee
FESBC	Forest Enhancement Society of British Columbia
FTIR	Fourier-transform infrared spectroscopy
G:O	Graphitic-to-Oxygenated Ratio
GHG	Greenhouse Gas
GO	Graphene Oxide
ICP-OES	Inductively Coupled Plasma Optical Emission Spectrometry
IR	Infrared
KP	Potassium Phosphate (K_3PO_4)
MESO	Mesoporous Zeolite

PV	Pore Volume
SEM	Scanning Electron Microscope
SRF	Slow Release Fertilizer
TGA	Thermogravimetric Analysis
TOS	Time-on-stream
UBC	University of British Columbia
WHC	Water Holding Capacity

Acknowledgments

I would like to thank my supervisor, Dr. Xiaotao Bi for taking me on as a student in his group and for always being available to offer support and guidance in my academics and future career. Thank you also to Dr. Anthony Lau and Dr. Loretta Li for offering their service as my committee members. A special thanks to Dr. Wei-Hsin Chen and his student's for welcoming me to Taiwan and supporting me during my visit to National Cheng Kung University.

I would like to thank my lab mates for listening to me ramble in group meetings and always offering their advice and support. Thank you to Bingcheng Lin for his support in helping me design my experiment and for his friendship. Thank you to Bill Cheng, Rachel Wang, and Mohammad Shanb Ghazani for their valuable technical support. Sincere thanks to Doug Yuen and the workshop staff for their continued help with equipment maintenance and to The University of British Columbia's Centre for Sustainable Food Systems at the UBC Farm, located on the traditional, ancestral, and unceded territory of the Musqueam people.

I would finally like to thank my friends and family: Zeid, David, Christine, Seoeun, and Mohammad who have given me lasting memories from Vancouver; Shannon, Jade, and Vanessa who have always been there to listen and to laugh; my parents who have endured countless dinner-time phone calls; my siblings who I'd be lost without; and to my partner Jesse who makes anywhere my home.

Chapter 1: Background

1.1 Woody Biomass in BC

British Columbia (BC), Canada is covered in a vast 55 M hectares of forest, making up 60% of the provinces total area [1]. Much of this forest area can be sustainably used as a resource in BC's timber industry. Some, however, are not of timber grade ('wood residues') and other uses are being sought, including use as a source of fuel or alternative product. These residues are then considered 'biomass'.

According to a 2019 University of British Columbia (UBC) study, 25.7 Mm^3 of wood matter in BC is currently left unused or wasted and is available as a biomass resource. These sources include: [2]

- Trees attacked by the Mountain Pine Beetle: totaling an estimated 752 Mm^3 (58%) of merchantable pine trees and a resulting $57 billion loss over 30 years [3], [4].
- Harvest residues: 11% of timber that is harvested is not of timber grade.
- Sawmill residues: 16% of timber input to sawmills are unusable and often wasted.
- Sanding timbers: BC issues a 'sustainable allowable cut region' each year, in which not all timbers are harvested. Leftover trees in these regions can therefore be used as a source of biomass [2].

Globally, the use of biomass from wood waste sources has been of growing interest as it reduces the reliance on virgin materials and contributes toward a circular economy. To support the use of wood residues from low value forests, the Forest Enhancement Society of British Columbia

(FESBC) is working with companies throughout the province, and in 2019 funded $233 M to 250 projects [5]. The growth of these projects and future research is vital to optimize the use of wood residues, for cost effective and sustainable replacement of virgin materials.

1.2 Influence of Canada's Increasing Crop Demand

Canada's population growth rate was estimated at 1.4 % in 2018, the highest among all G7 countries [6]. From this population growth comes a greater demand for food. The production of wheat and grain, for example, is expected to increase by 5 and 8%, respectively, in only two years (2019 – 2021) [7]. With increased crop production comes increased use of fertilizers. In Canada, the use of nitrogen (N_2) and phosphorous (P) fertilizers have increased continually since 1980 [8]. Generally, fertilizers are added to soils to increase concentrations of N_2, P, and potassium (K). If they are added in excess though, they can lead to greenhouse gas (GHG) emissions, groundwater contamination, or soil acidification [9], [10]. Fertilizers that are quick to leach into water must be replaced often, leading to further contamination and high expenses. To reduce fertilizer release rates, coating materials such as polymers, sulphur and clays have been used as a physical barrier surrounding the fertilizer beads ('controlled release' fertilizing). However, they can often be toxic, polluting, or slow to degrade. Certain carbon-based coatings are of current interest as they can both slow the nutrient release rate and be permanently sequestered underground, preventing harmful emissions to the atmosphere [9].

Furthermore, an increased crop demand inevitably leads to a portion of the produce left as residual waste. Under certain soil conditions, these residues can be tilled back into the soil. However, for soil too dense or wet, such as the clay-type soils in central Canada, the residues cannot be tilled, leaving burning as an alternative and releasing harmful carbon dioxide (CO_2) [11].

As a burning alternative, the pyrolysis process could be used to convert the crop residues into biochar, a carbon-dense, porous material which can be added back into crop soils. Biochar in soils can both retain fertilizer nutrients and sequester the carbon underground, preventing the CO_2 emissions that would be released from burning or natural degradation [9], [12]

The use of wood and/or crop residues to produce biochar for agriculture purposes is a practice contributing to a circular economy by replacing the reliance on 'taking', 'making', and 'disposing', leading to both environmental and economic benefits [13].

1.3 Biomass and Pyrolysis

Biomass can be thermochemically converted into renewable products of biochar, biooil, and syngas, with applications ranging from soil remediation to transportation fuels. Biogenic carbon emitted from breaking down plant-source biomass is considered net-zero; if it were not thermochemically converted, it would have naturally decomposed into CO_2. This CO_2, whether released through thermochemical or natural decomposition, will again be sequestered into living plants via photosynthesis. By comparison, burning fossil fuels for energy production introduces anthropogenic carbon in the form of CO_2 into the atmosphere from deep underground stores [14].

1.3.1 Woody Biomass

Woody biomass is primarily composed of cellulose, hemicellulose, and lignin, with typical dry wood compositions of 45, 30, and 25 wt%, respectively (Figure 1). Cellulose is made up of a series of ridged chain structures aligned as a linear polymer. It typically degrades at temperatures between 240 – 350 ^{o}C. Hemicellulose, however, is comprised of monosaccharide molecules, such as glucose, galactose, and manose, chained together in a polymer structure. It typically decomposes

between 200 – 260 ^{o}C. A greater composition of hemicellulose typically yields more volatiles and less biochar. Finally, lignin has an amorphous structure with many irregular branches, sometimes decomposing at temperatures as high as 500-900 $^{\circ}$C [15], [16].

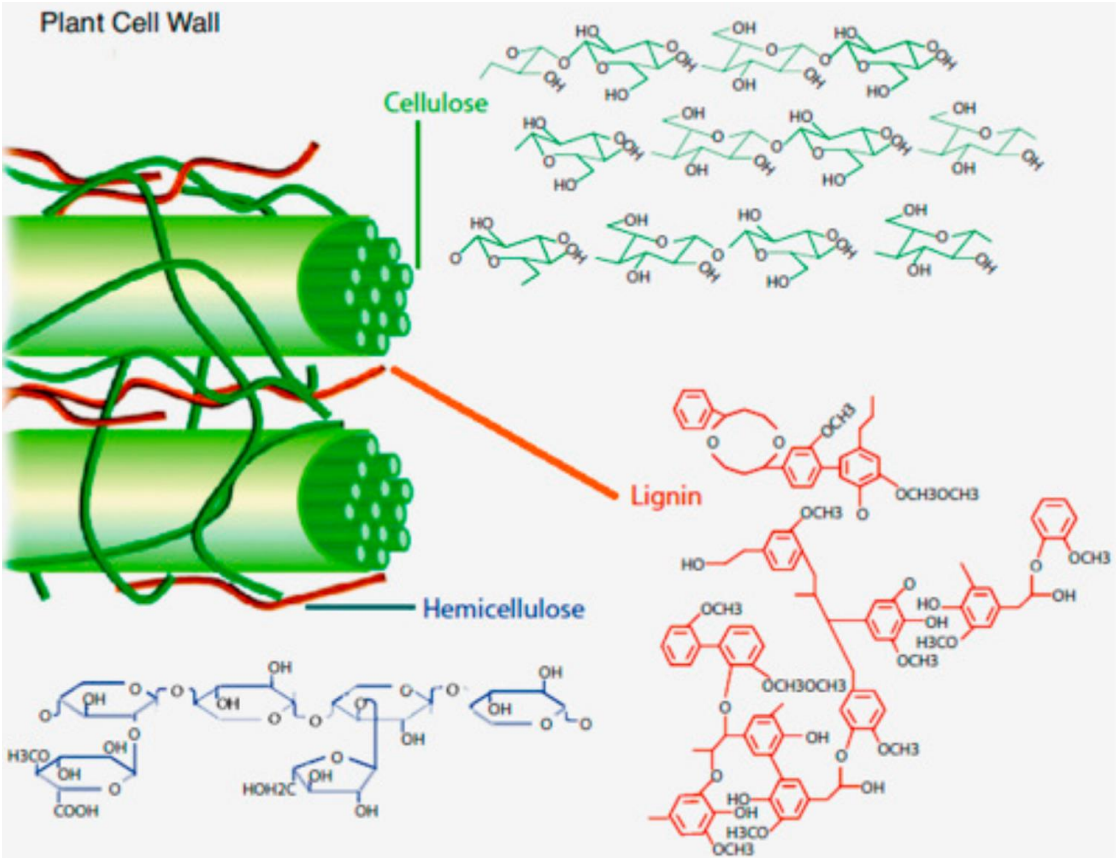

Figure 1: Cellulose, hemicellulose, and lignin in a plant cell wall from [17]

Pyrolysis decomposition curves of wood are shown in Figure 2, showing that that hemicellulose and cellulose were the easiest to decompose, while lignin degraded over the entire temperature range (100 – 900 ^{o}C), due to its wide range of molecular constituents. The remaining solids after pyrolysis were greatest from lignin, at 45 wt% [18].

Figure 3 compares the pyrolysis and combustion curves of wood, showing that pyrolysis displays only one decomposition stage, whereas combustion displays two: the first from the

combustion of cellulose and hemicellulose and partial lignin, and the second from combustion of the remaining lignin and some oxidation of chars [19].

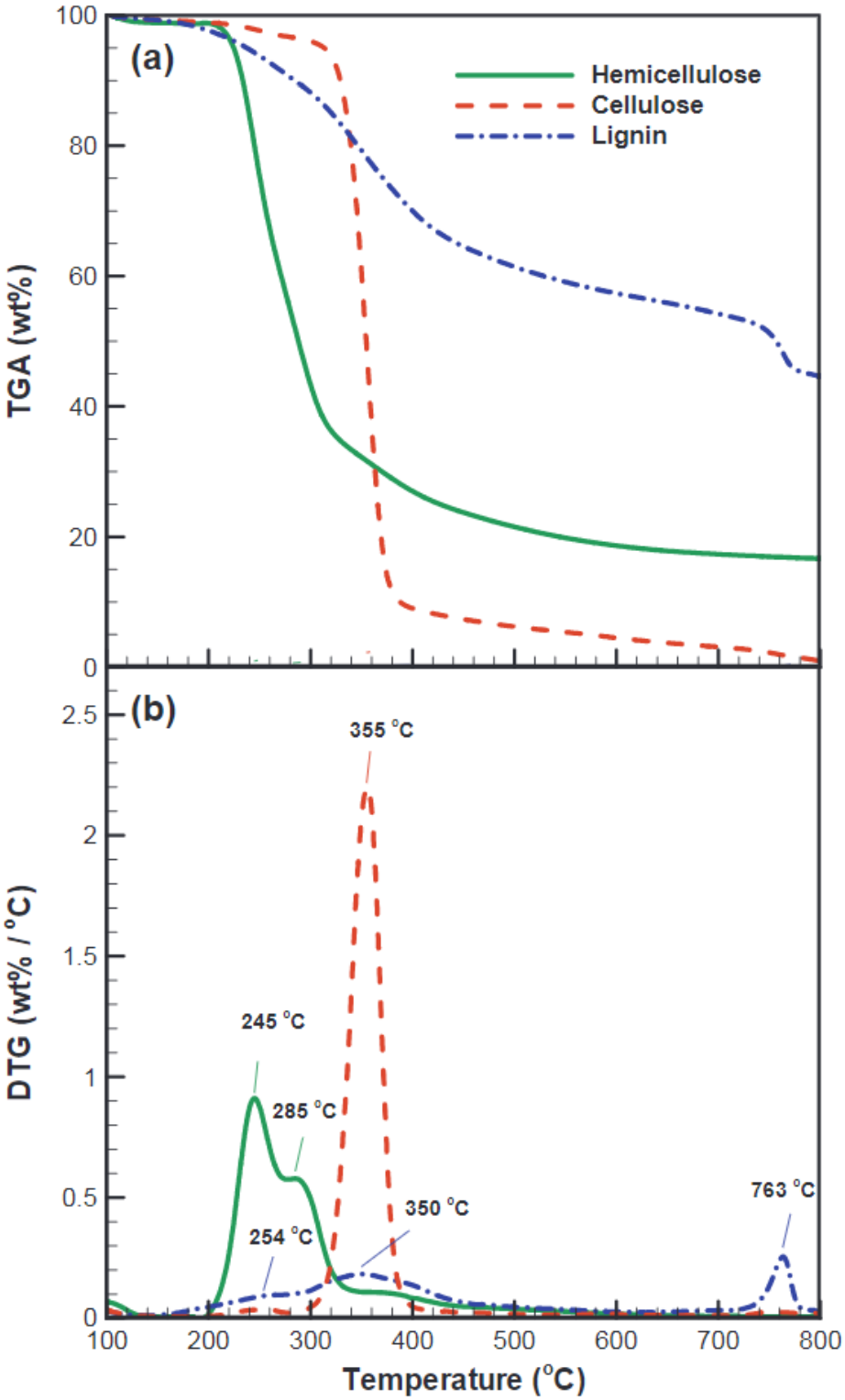

Figure 2: Pyrolysis decomposition thermogravimetric analysis (TGA) and derivative TG (DTG) curves of wood from heated at 10 ºC/min in N_2 from [18]

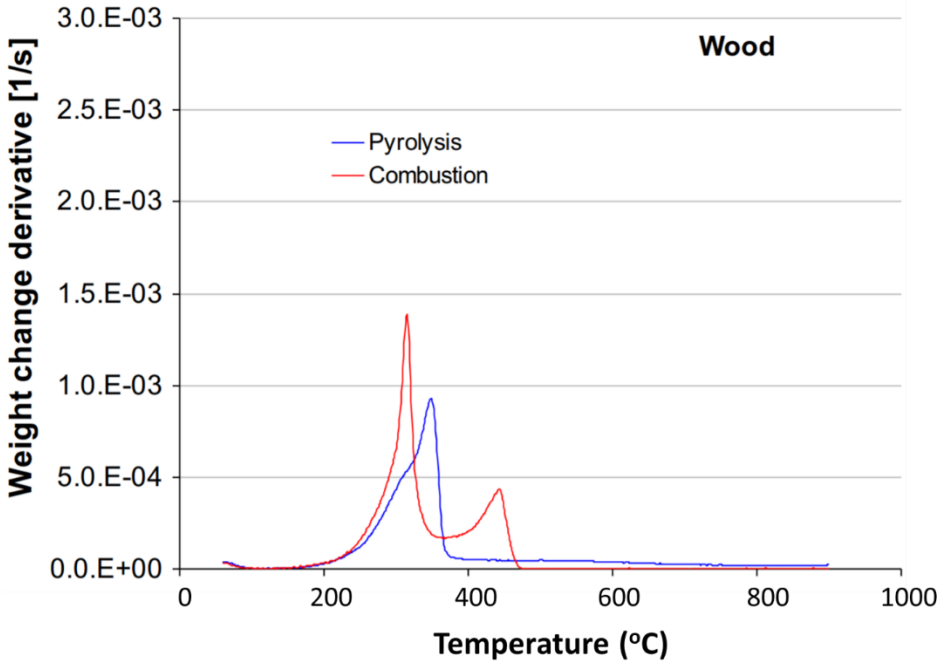

Figure 3: Pyrolysis and combustion DTG curves of wood heated at 5 C/min in argon (pyrolysis) or oxygen to argon ratio of 21:79 (combustion) from [19]

1.3.2 Pyrolysis

Pyrolysis has gained much recent attention in research as a thermochemical conversion method for biomass utilization. Pyrolysis breaks down biomass under temperatures between 300 – 700 °C in the absence of oxygen. The oxygen-free environment prevents combustion reactions, therefore limiting CO_2 production and diversifying the product yield, allowing production of biochar, biooil, and non-condensable gases [20]. Pyrolysis is typically categorized as slow, fast, or flash pyrolysis, depending on the process heating rate and temperature. The process conditions greatly influence the product yields. Generally, as the process heating rate and temperature increases, the yield of biochar decreases as the bound volatiles escape to produce biooil and non-condensable gases [14], [20]. Typical conditions and product yields are shown in Table 1.

Table 1: Conditions and product yields typical of pyrolysis processes from [14], [20]**.**

Process	Residence time (s)	Heating rate (°C/s)	Particle size (mm)	Temperature (°C)	Product yield (%)		
					Oil	Char	Gas
Slow	450 – 550	0.1 – 1	5 – 50	450 – 650	30	35	35
Fast	0.5 – 10	10 – 1000	<1	450 – 600	50	20	30
Flash	0.3 – 1.5	>1000	<0.2	600 – 1000	75	12	13

Biooil

Bio-oil production is favored in processes with low to moderate temperatures, high heating rates, and short gas residence times. It is collected via rapid quenching of the vapour phase to separate liquids from non-condensables. Bio-oils have not yet reached commercial crude oil standards for upgrading but have the potential to replace fossil fuels in heat, power, and chemical applications [14]. Table 2 lists several advantages and disadvantages of bio-oil as fuel. Bio-oil is prone to increase in viscosity during storage due to polymerization reactions [20]. Bio-oils also have a very high oxygen content, often as high as 50 wt%. Many negative bio-oil properties are attributed to the high oxygen levels, such as its high polarity, high acidity, low stability, and low energy density in comparison to fossil fuels. Currently, hydrodeoxygenation seems to be a promising method of oxygen removal. However, this method requires a supply of large amounts of high-pressure oxygen, as well as a large plant facility, which lead to high capital and operation costs [21], [22].

Table 2: Advantages and disadvantages of bio-oil as a fuel [14], [21], [22]

Advantages	Current Limitations
• Environmentally sustainable • Potential use in existing power plants • Higher energy density than biomass gasification fuel • Liquid fuels have easier storage and transportation than solids	• Higher CO emissions than diesel during combustion • High viscosity • High water content • Susceptible to fouling • Low stability

Non-condensable gases

Non-condensable volatiles are derived from cracking of volatiles released from biomass decomposition. They are composed largely of small-molecule hydrocarbons, carbon monoxide (CO) and hydrogen (H_2), with fractional amounts of CO_2, water vapour, and nitrogen (N_2), and trace amounts of heavy hydrocarbons (tar), and ash. The presence of CO and CO_2 prove that partial oxidation takes place through the oxygen present in the biomass feedstock. Generally, increased pyrolysis temperatures and heating rates lead to greater thermal degradation and devolatization rates, increasing the gaseous yield [14], [20]. A portion of the gasses sensible heat can be used for steam generation for heat and power, while some low-molecule hydrocarbons, H_2 and CO can be used as feedstock for chemical industries [20].

Biochar

Biochar (or charcoal) is the carbon matrix left behind when the volatile components are removed from biomass in an oxygen-limited environment. The term biochar is used when the product is to be used for soil amendment and environmental remediation. Charcoal, however, refers to the product as a fuel for cooking or heat generation. Lower pyrolysis heating rates

typically favour biochar production over biooil and gases, as the volatiles remain bound to the solid carbon via condensation/repolymerization. Larger biomass particle sizes have also been proposed to limit devolatization rates, thus increasing the overall biochar yield [12], [20].

When added to soil, the high surface area of biochar has been suggested to increase soil aeration, water holding capacity, plant growth, and soil workability [12], [23], [24]. It has also been suggested to have a high cation exchange capacity (CEC), allowing it to bind cations (such as K^+ and NH_4^+ from fertilizers) within the soil, making them more available for plant uptake, and limiting their leaching potential [12], [25]. A high CEC also allows biochar to immobilize heavy metal cations in contaminated soils and prevent spreading [24].

Biochar is an extremely stable compound, lasting millennia before decomposing. This makes it extremely attractive as a carbon sink; biochar buried in soils will stay buried, preventing carbon release into the atmosphere. The use of pyrolysis to produce biochar for soil amendment therefore has several benefits: (1) soil improvement, (2) use of decaying trees from low value forests, (3) carbon sequestration, and (4) coupled renewable energy production (if produced with biooil and/or gases for fuel) [12] [25].

Potassium Phosphate in Pyrolysis

Potassium phosphate (K_3PO_4) contains both potassium (K) and phosphorous (P), and both suppress the formation of levoglucosan: a monomer from the decomposition of cellulose, and a precursor to volatile formation [20], [26]–[30], thus increasing the overall biochar yield in pyrolysis and decreasing the bio-oil yield. K_3PO_4 was also found to inhibit the devolatization of hemicellulose, increasing the biochar yield. Of the biooil that is produced, the acidity decreases remarkably and the phenolic content greatly increases (Table 3) [31], [32]. The use of K_3PO_4 also

increases the Brunauer–Emmett–Teller (BET) surface area of biochar; with catalyst loadings of 20 wt% in switchgrass the BET surface area increased by 56 % when K_3PO_4 was used over a clinoptilolite catalyst [32]. This leads to improved water retention and nutrient adsorption when added to soils.

Table 3: Product composition of biooil produced from microwave pyrolysis of switchgrass with and without K_3PO_4, (peak area % analyzed using GC-MS) [32]

Feedstock	Acids	Phenolics	Furans	Ketones	Aldehydes	Anhydrosugars
Switchgrass	24.6	11.0	4.81	16.5	1.23	0.63
Switchgrass + 30 wt% K_3PO_4	5.95	45.4	1.15	7.12	0	0
Percent change (%)	-76	+312	-76	-57	-100	-100

Chapter 2: Introduction to Microwave Pyrolysis

2.1 Microwave Pyrolysis

Conventional pyrolysis is carried out in reactors heated electrically through the exterior. The heat transfers through the reactor via conduction and among the reactor wall and particles. The heat conduction, however, is limited by the conductivity of the feedstock particles which is usually quite low for dry organic matter. Microwave heating has been proposed as a method to improve the heat transfer during pyrolysis, with the potential to heat particles locally more rapidly and more uniformly [33], [34]. Microwave irradiation can penetrate the particles in the reactor (rather than just the exterior). Simple cross-sections of both conventional- and microwave-heated reactor profiles are shown in Figure 4.

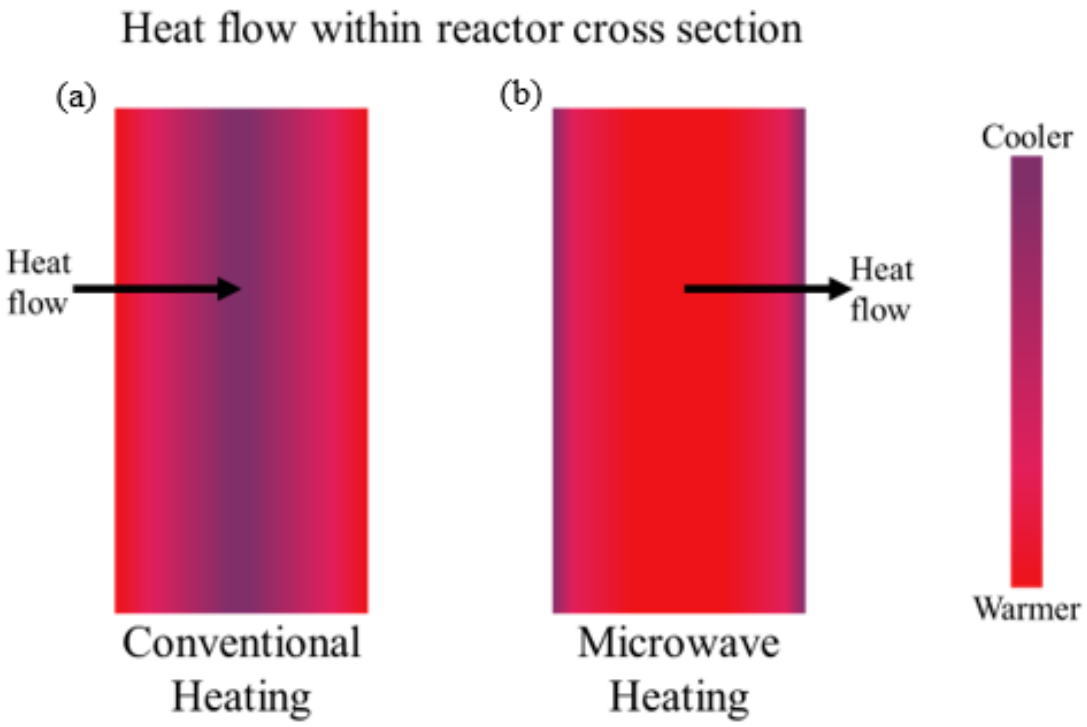

Figure 4: Heat flow in reactor cross-section - (a) conventional externally heated and (b) microwave heated with an in-situ absorber, adapted from [33], [34]

In the case of microwave irradiation, heating is limited by the microwave absorbance of the feedstock materials. Microwaves heat substances differently based on their material type. In the case of polar compounds (i.e. water-containing foodstuff), the microwave field radiating toward the substance causes the dipoles within it to align with the oscillation of the field. This produces molecular friction and thus heat (dipolar polarization). In the case of ionic solids with mobile electrons (i.e. mobile pi-bonded electrons in sp^2 carbon-bonded materials), the microwave field induces a current of electrons which release energy in the form of heat via the 'Maxwell-Wagner-Sillars' effect [35].

The efficiency of a substance to release energy as heat is represented by the dielectric loss (ε"). Alternatively, the ability of a substance to store energy is represented by the dielectric

constant (ε'). The ratio of the two is called the loss tangent (tan δ = ε"/ ε') which provides a full quantitative measurement of a substance's ability to convert absorbed microwaves to heat (microwave absorbance); substances with a greater loss tangent have a high efficiency in converting microwaves to heat, heating rapidly and efficiently. A substance's loss tangent depends directly on its dielectric properties [36], [37]. The tan δ value of water at room temperature and 2.45 GHz compared to typical biomass feedstocks are given in Table 4.

Table 4: Typical tan δ values of water [37] and biomass feedstocks [38]

Material	tan δ
Water	0.123
Pine sawdust	0.0101
Live oak	0.0490
Tallow tree	0.0397
Biochar from pine sawdust	0.2903

Biomass materials that have a high microwave absorbance (pure lignin, biochar) can be heated directly by microwave. In these cases, biomass particles can absorb microwaves uniformly and efficiently, compared to conventional heating.

Lignocellulosic biomass, however, has a low microwave absorbance. Thus, 'microwave absorbers' (materials with a high tan δ) are commonly added to the biomass sample to improve microwave absorption and heating. In this case, the biomass is heated indirectly via conduction with the warmer microwave absorbers. Typical absorbers include silicon carbide (SiC) and biochar.

Potassium phosphate (K_3PO_4) has been used as a microwave absorber particularly for the production of biochar for soil application, as it (1) increases microwave absorbance, (2) catalytically increases the yield of biochar, and (3) adds K and P nutrients into soils downstream (Figure 5) [24]. Microwave heating has also been found to increase biochar porosity, a beneficial

property for soil application, compared to conventional electric heating [39], [40]. A comparison of typical characteristics of conventional and microwave heating methods for pyrolysis are listed in Table 5.

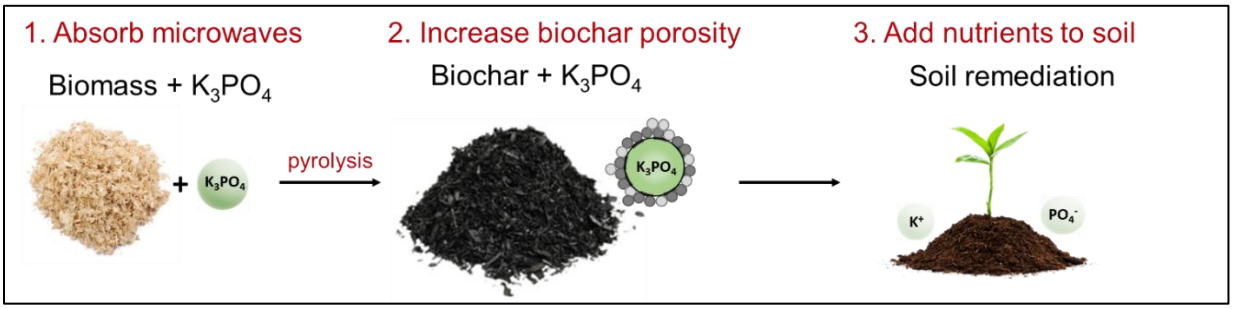

Figure 5: Added benefits of potassium phosphate

Table 5: Comparison of microwave and conventional heating for pyrolysis

Microwave heating	Conventional heating	Source
• Rapid heating	• Slow heating	[34], [41]
• Material-selective heating	• Nonselective heating	[34], [41]
• Uniform particle heating	• Non-uniform particle heating	[34], [41]
• Microwave absorber usually required	• No additive required	[34], [41]
• Lower biooil yield	• Greater biooil yield	[42]
• Higher biochar surface area	• Lower biochar surface area	[40]

Microwave pyrolysis has been suggested to increase endothermic gasification reactions compared to conventional pyrolysis. In a microwave reactor, the sample is heated internally and rapidly such that any internalized water vaporizes before exiting the reactor. These hot vapours, along with other pyrolysis gases, react with the organic sample to favour the endothermic gasification reactions, shown below in reactions (1) and (2). In conventional pyrolysis, however, the sample particles are heated at a slower rate allowing more time for reactions between non-condensable gases and for cracking reactions to increase the hydrocarbon content in the pyrolysis vapours, thus favouring reactions (3) and (4) [43].

$$C + H_2O \leftrightarrow CO + H_2 \qquad \Delta H_{298} = 132 \text{ kJ/mol} \quad (1)$$

$$C + CO_2 \leftrightarrow 2CO \qquad \Delta H_{298} = 173 \text{ kJ/mol} \quad (2)$$

$$CO + H_2O \leftrightarrow CO_2 + H_2 \qquad \Delta H_{298} = -41.5 \text{ kJ/mol} \quad (3)$$

$$CO + 3H_2 \rightarrow CH_4 + H_2O \qquad \Delta H_{298} = -206 \text{ kJ/mol} \quad (4)$$

2.2 Pyrolytic Coke

'Coking' is the process associated with the formation of fine, carbonaceous particles in layers around a nucleus site, such as a catalyst. Coke forms from almost all hydrocarbon upgrading reactions and is conventionally seen as a process disadvantage as it can block catalyst pores and acid sites, causing it to deactivate. Regeneration of a deactivated catalyst requires an additional process step at high temperatures and risks further catalyst damage [44], [45]. It is challenging to prevent the catalyst from coking as the process mechanism is not yet well-understood and differs greatly between feedstocks and process conditions. In biomass pyrolysis for biochar production, however, the catalyst can remain with the biochar product for soil application, eliminating the need for a catalyst regeneration process.

Coke is generally divided into two primary types: oxygenated coke and graphitic coke. Oxygenated coke has an amorphous structure, consisting of sp^3-bonded carbons attached to oxygen-containing functional groups. Under certain reaction conditions, the oxygenated coke is dehydrogenated, transformed into graphitic coke, a very stable, carbon-rich compound. It has a polyaromatic structure, consisting of sp^2-bonded carbons with no functional groups, as they are cleaved off during the dehydrogenation step (Figure 6) [44]–[46]. However, to use this graphitic coke by-product as an effective microwave absorber, it is necessary to understand the pyrolysis conditions under which its production is favoured over oxygenated coke – a subject which is currently not well understood in the literature.

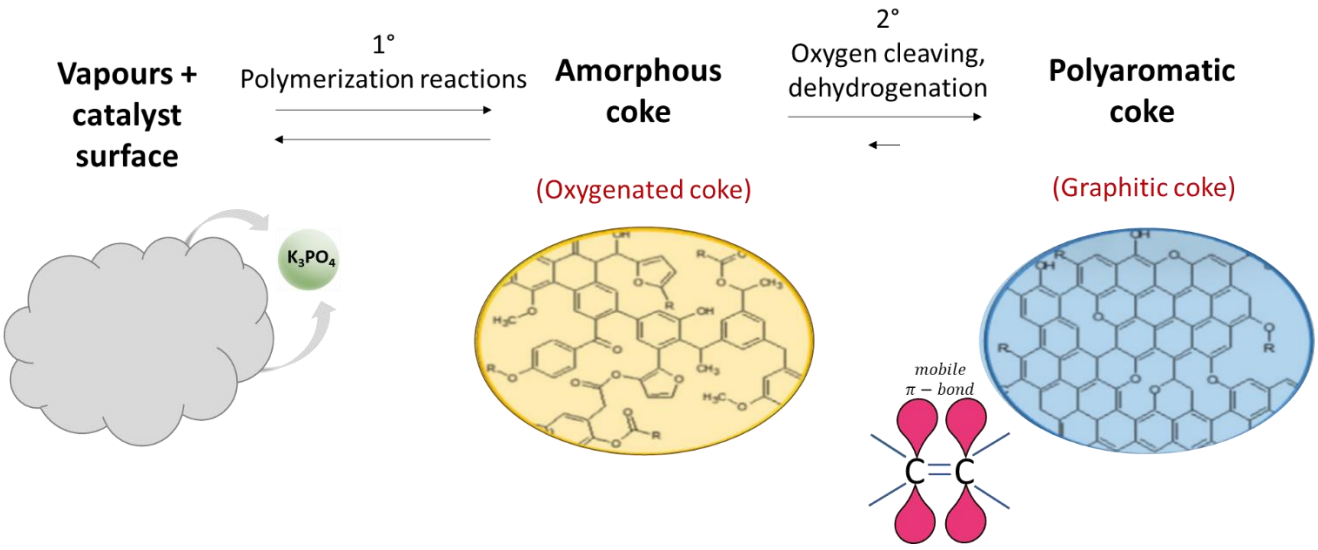

Figure 6: Formation of coke from pyrolysis vapours, adapted from [47].

2.2.1 Temperature Effect

It is agreed among researchers that the coking reaction mechanism changes with the reaction temperature, thus, affecting the coke yield and type of coke. Some reported a trend in which the coke yield experiences a minimum around 400 – 500 °C, for a propene-zeolite reaction and an FCC reaction [45], [48]. In contrast, coke yield has been observed to decrease at increasing temperatures, with its surface becoming rough as decomposition intensifies [49]. These observations differ from others in which the coke yield increases continually with increasing temperature [50], [51]. The temperature effect on the coking rate and yield is summarized in Table 6.

Experiment	Temperature effect	Source
Upgrading bio-oil with ZSM-5	> 400 °C – Substantial increase in coke formation	[50]
Hydrodesulphurization catalysts	< 375 °C – High coking rate 375 – 440 °C – Slow coking rate due to hydrogenation reactions > 440 °C – High coking rate due to dehydrogenation reactions	[52]
FCC of light crude oil	Coke yield increases with temperature, 650 °C – highest coke yield observed	[51]
Coking in FCC riser	455 °C – High coke yield due to carbon free radicals not desorbing 500 °C – Minimum coke yield 555 °C – High coke yield due to olefin polymerization	[48]
Propene transformation over HMFI zeolite	400 °C – Coke yield passes through a minimum	[45]

Table 6: Effect of reaction temperature on coking rate and yield

The reported temperature dependency on the type of coke is also not consistent between sources, but overall it seems that at higher temperatures the coke is densely carbonaceous and likely graphitic [45]. With increasing temperature, the oxygen-containing functional groups within coke may become unstable and crack [48]. These cracking reactions seem to form a graphitic structure at temperatures as low as 200 °C [53], or more commonly reported as above 330 °C [44], [45], [54], [55]. This is summarized in Table 7.

Table 7: Effect of reaction temperature (T) on the type of coke

Experiment	Temperature effect	Source
Biooil catalytic hydrogenation with Ni/HZSM-5 in fixed bed autoclave	250 – 280 °C – Coke contains olefins and double-bonded hydrocarbons 280 – 300 °C – Dehydrogenation begins, aromatic coke formation begins 300 – 330 °C – Coke contained alkyl and polycondensed aromatics (graphite)	[44]
Catalytic cracking of hydrocarbons with zeolites	< 200 °C – 'Low T coke I', olefins, diolefins, and alkanes > 350 °C – 'High T coke II', methylpolyaromatics Longer time-on-stream increases the fraction of coke II	[45]
Catalytic cracking of furan with H-ZSM-5 in a fixed-bed reactor	< 200 °C – Coke is aliphatic > 200 °C – Coke is polyaromatic A significant drop in OH groups when T increased from 200 – 300 °C, then remained constant from 300 – 600 °C.	[53]
Thermocracking from heating heavy oil – no catalyst	< 300 °C – Light hydrocarbons begin to evaporate 300 – 350 °C – Aromatic coke begins to form 350 °C – Coke formation is almost complete 400 °C – Oxygen functional groups are further cleaved off	[54]
Pyrolysis of bio-oil – no catalyst	Carbon-content increases (60 – 80%) at higher temperatures (300 – 800 °C)	[55]

Temperature Effect on Biochar Properties

Along with coke, biochar properties are also greatly affected by changes in pyrolysis conditions which in turn affect its ability to hold nutrients and water when added to soil. The CEC of sawdust biochar decreased (from 56.13 to 39.22 Cmol/kg) and the BET surface area increased (from 3.39 to 443.79 m^2/g) as the pyrolysis temperature increased (350 – 650 ^oC). The CEC is an indicator of how well the biochar can hold onto cations (nutrients like K^+) in the soil. Therefore, lower temperature biochar has an improved ability to prevent cation leaching in soils. The BET surface area, however, is a good indicator of how well biochar can retain water within soils: a

larger BET surface area can retain a greater volume of water. Therefore, higher reaction temperatures (and thus larger surface areas) are expected to increase the water holding capacity (WHC) of biochar when added to soil [56]. Since increased temperatures have a much greater positive effect on BET surface area (130 % increase) and a much smaller negative effect on CEC (30 % decrease), it is likely that, when added to soil, high-temperature biochar can improve the soil properties more than low-temperature biochar.

2.2.2 Heating Rate Effect

The oxygen content in coke seems to decrease with slower heating rates, likely because slower heating rates allow enough time for oxygen-containing functional groups to crack [55]. The coke yield has also been studied over a broad heating range (1-1000 °C/s) during catalytic fast pyrolysis of glucose with ZSM-5 and was found to decrease from about 40% to 35% with increasing the heating rate [57]. It seems then that slower heating rates promote both a higher yield and a greater degree of graphitization of coke.

2.2.3 Catalyst Type Effect

The physical properties of the catalyst seem to influence the total coke yield: coke yield increases with acidity and density of active sites, and with the size of catalyst pores [45], [51]. The effect of catalyst-to-feed ratio on the coke yield is not agreed upon by researchers [45], [51], [58]. The coke yield during fast pyrolysis of glucose was compared using different catalysts with a broad range of properties to isolate the effect of each property on the yield [57]. The results (summarized in Table 8) show a clear difference in coke yield, but do not provide any clear trend between the catalyst properties and yield.

Table 8: Catalyst property effect on coking yield [57]

Catalyst type	Catalyst properties	Coke yield (%)
ZSM-5	• Bronstead acid sites • Same pore structure as silicate • Intersecting pore channels	35%
Silicate	• No Bronstead sites	40%
Y-zeolite	• 3-D pore structure	50%
B-zeolite	• Intersecting channels	70%
Silica-alumina	• Contains Bronstead sites • Amorphous	85%

There are some insights, however, on how the catalyst active species affects the type of coke. When nickel (Ni) active sites were compared to nickel-copper (Ni-Cu) active sites on a zeolite catalyst, the plain Ni produced a greater amount of coke, and a greater fraction of polyaromatic (graphitic) coke. The addition of Cu was suggested to improve Ni dispersion and particle size, decreasing the contact time between oxygenated species and the Ni, limiting polyaromatic coke formation to the same extent [44]. In a separate study, La_2O_3 was added to a zeolite catalyst and compared to the plain catalyst. The La_2O_3-modified catalyst changed the overall pore size and acidity which led to a decrease in the overall amount of coke and fraction of polyaromatic coke [46].

2.2.4 Coke and Microwaves

Microwave irradiation was used to examine the amount and type of coke during a 5-hour methanol-to-hydrocarbon reaction over a nano H-ZSM-5 zeolite catalyst (Si/Al ratio 160) in a down flow reactor. The resulting coke was separated based on its position in the reactor (top or bottom). It was found that top-coke was mainly aromatic (graphitic coke) while bottom-coke was

mainly aliphatic (oxygenated coke), supported by TGA and Raman spectroscopy. The aromatic coke had a much greater microwave absorption efficiency (normalized by coke weight, ε”/wt%) than the aliphatic coke (0.135:0.02) (Figure 7a). The same trend was observed with zeolites of different Si/Al ratios (of 46 and 60).

The researchers also studied the effect of retention time on the microwave absorption of coke but found that its effect depended on the type of catalyst used. Surprisingly, the greater retention time decreased the microwave absorption (and thus polyaromatic coke) when a nano zeolite (ZSM-5, Si/Al ratio of 25) catalyst was used. Figure 7b compares the nano zeolite to a mesoporous zeolite (MESO 40-60). Raman spectra results from the longer time (5h) coked sample showed more poly-olefinic species than polyaromatics, thus causing the decrease in microwave absorbance [49].

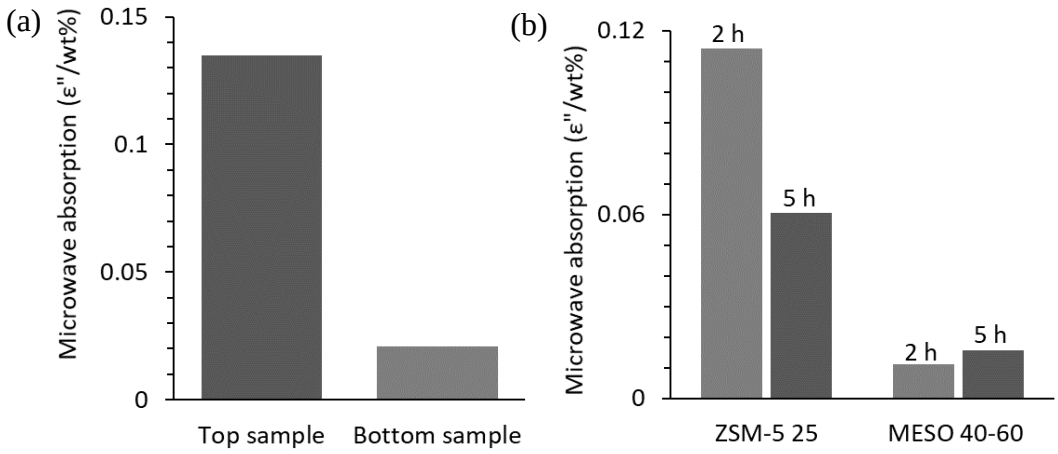

Figure 7: Microwave absorption of coked catalysts: (a) effect of sample location in reactor and (b) effect of retention time, adapted from [49]

2.3 Fertilizer Coatings

2.3.1 Potassium Phosphate as a Fertilizer

Fertilizers are classified by their N:P:K values, always adding to 100. The N:P:K ratio of potassium phosphate is 0:33:67. It would be beneficial to soils already rich in N_2 or as an additive to N-rich fertilizers. As a fertilizer, it is offered as a powder or granules.

2.3.2 Controlled-Release Fertilizers

To prevent excess nutrients (N,P,K) from leaching into soils from fertilization, controlled release fertilizers (CRFs) are of heightened interest. This is still a developing technology, although it has existed for several decades. In 1997, CRFs were defined as fertilizers which could delay the availability of nutrients to plants after application, significantly longer than a 'rapidly available fertilizer' [9], [59], [60]. More recently, however, there have been recommendations in terminology of these fertilizers, specifically in differentiating CRFs from slow-release fertilizers (SRFs). Generally, CRFs refer to fertilizers which have controllable and predictable release patterns based on the soil properties. SRFs, however, refer to the fertilizers which delay the nutrient release compared to rapidly available fertilizers, but their release pattern is not predictable and depends largely on the soil properties. According to Sempeho et al. (2014) the European Standardization Committee (ESC) declared that fertilizers can be considered CRFs if they release at least 15% of their nutrients by 24 h at room temperature, but no more than 75% after 28 days [61].

The release of fertilizers is generally slowed in one of two ways (1) using a fertilizer of low solubility, and (2) covering the nutrient with a physical barrier. Fertilizers of low solubility include

organic materials such as animal manure or sewage sludge, or inorganic materials such as metal ammonium phosphates. Fertilizers with a physical coating barrier are typically in the form of granular pellets, each pellet covered in a coating layer. The layer slowly releases the nutrient within when in contact with water, via diffusion; water enters the coating layer and nutrients diffuse out of the layer with time. If, however, the water within the coating layer builds the osmotic pressure too high, the coating is at risk of bursting, causing a 'failure mechanism'. Weak coating barriers, such as sulfur-based coatings often exhibit a failure mechanism, whereas polymer coatings tend to show nutrient diffusion [62]–[64].

Common coating types are listed in Table 9. Research is emerging on the use of biodegradable polymers for CRFs, with the potential benefits of polymer coatings (simple mechanism, adjustable control), but with low risk of pollution and toxicity. However, more work is needed before these become widely used commercially [9], [64], [65].

Table 9: Advantages and disadvantages of common coating types [9], [64], [65]

Coating Type	Advantages	Disadvantages
Sulfur-based	• Biodegradable	• Sensitive to soil conditions • Irregular release
Nondegradable polymers	• Adjustable control with thickness and coating process • Hydrophobic • Simple coating mechanism	• Risk of toxicity • Costly
Biodegradable polymers	• Low cost • Low environmental risk	• Weak coating barrier • Hydrophilic • Modification needed

Furthermore, since K_3PO_4 acts both as a nutrient source and as a microwave absorber to produce biochar for soil amendment, coke formation on the surface of K_3PO_4 has the potential to act as a barrier to control the release of K^+ and PO_4^- into soils. Coke has not been tested as a coating

layer ever before. However, graphene oxide films have a similar composition to coke as structured carbon sheets containing some oxygen functional groups. The films have been mechanically coated onto fertilizer pellets to delay release up to 10 days [60], [66]. Biooil has also been used as a spray-coating for fertilizer pellets [67]. The use of these carbon-coated fertilizers is listed in Table 10.

Table 10: Summary of literature on carbon-based fertilizer coatings

Materials	Coating method	Release effect	Source
KNO_3 pellets coated with graphene oxide (GO) films	GO paper was dissolved in solution and filtered through a membrane. The resulting GO film was peeled from the membrane and mechanically coated into KNO_3 pellets. The GO film had few oxygen functional groups after heat treatment with KNO_3.	K^+ release in water was measured over 10h, with 35 % release in 7h, followed by a burst of 94 % released after 8h, likely due to cracks in the film.	[66]
KNO_3 beads coated with chitosan and GO (CS-GO) films	KNO_3 beads were submerged into CS-GO solutions, removed, and submerged into NaOH solutions. A shell formed around the beads which were then left to air dry. The coating was about 30 wt% of the resulting fertilizer.	K^+ release in water was measured over 10 days, showing about 80 % release by day 5.	[60]
Biochar + N,P,K mixtures spray-coated with biooil	Biochar was mixed with KH_2PO_4 and KNO_3 solution and dried, then spray coated with biooil.	The nutrient release after 7 days of soil incubation was only about 40%. The biooil coating has a greater effect in delaying the release of phosphorus than potassium.	[67]

2.4 Research Objectives and Tasks

The following research questions are posed:

1) How do microwave pyrolysis reaction conditions affect the type of coke and coke yield with the use of a K_3PO_4 catalyst?
2) How does the coke formation (type and yield) affect the microwave absorption during pyrolysis?
3) How does the coke formation (type and yield) affect the release rate of K_3PO_4 into soil post reaction?

Based on the literature review, the following hypotheses are formed in reference to the above questions:

1) Coke will become more graphitic (less oxygenated) as the reaction temperature is increased from 350 ^oC to 550 ^oC and the coke yield will increase as the reaction time is increased from 30 min to 50 min. A coke yield of approximately 30 wt% of the coked K_3PO_4 is expected [68].
2) The loss tangent, tanδ, of coked K_3PO_4 will be greater than fresh K_3PO_4, increasing more with degree of graphitzation and with coke yield. Coked K_3PO_4 recycled back into the pyrolysis reaction will help the microwave heating of the feedstock to a higher temperature than fresh K_3PO_4 when operated under the same microwave power.
3) Coked K_3PO_4 will leach slower through soil than fresh K_3PO_4. Coke produced at low temperatures (350 ^oC) will likely slow the release further by improving the cation exchange capacity with the presence of more oxygen functional groups.

The research tasks to be carried out are then:

1) To study the effect of microwave pyrolysis conditions (temperature and reaction time) on coke type and yield. Coke type and yield will be characterized using Raman Spectroscopy, thermogravimetric analysis (TGA), scanning electron microscopy (SEM), and elemental analysis (EA).
2) To recycle the coked catalyst to enhance microwave absorption. The coked catalyst will be re-mixed with fresh sawdust for pyrolysis, and the maximum achievable temperature will be recorded.
3) To measure the fertilizer release rate of coked K_3PO_4 under different coking conditions in comparison to fresh K_3PO_4.

Chapter 3: Materials and Methods

3.1 Experimental Feedstock

The biomass feedstock used was Douglas Fir sawdust supplied from Tolko Industries, Ltd. (Vernon, Canada). The sawdust was blended in a kitchen blender and separated into particles 300 – 600 μm in size. The prepared sawdust was dried overnight in an oven at 105 ^{o}C.

The potassium phosphate tribasic, anhydrous (K_3PO_4), was supplied from Sigma-Aldrich Canada Ltd. K_3PO_4 is a fine white powder (resembles flour) which absorbs water from air extremely quickly if not in a sealed container. Care was taken to prepare samples quickly to minimize water absorption.

Silicon carbide (carborundum boiling granules, SiC) were supplied by Thomas Scientific in #12 mesh size. Pellets were used rather than a powder to ensure that they could be separated by size from the post-reaction biochar product.

The soil used is from a covered hoop house at UBC farms collected by technician Tim Carter on 2020-10-06. The soil type is Bose Soil (from plot code NHH), described elsewhere [69]. The hoop house is typically fertilized using compost once or twice a year and is irrigated using city water through both overhead and drip methods. The crops grown in this soil include tomatoes, cucumbers, alliums, mustards, spinach, and carrots. The soil was collected at least 3 days after irrigation. The soil moisture content was measured to be 20 wt%. The void fraction of the fresh (not dried) soil was measured to be 40 vol%.

3.2 Experimental Apparatus

The microwave pyrolysis unit consists of a microwave oven (manufactured by EnWave Corporation, Vancouver, Canada), a waveguide directing the microwaves toward the reactor, a quartz tube reactor (manufactured by Technical Glass Products Inc., Ohio, USA) with a 44 mm inner diameter and 245 mm height, a data collection system, and a microwave leakage detection system.

Microwaves are generated at 2.45 GHz and guided through the transmission duct (waveguide) toward the quartz tube reactor. A water-cooling system ensures that all microwaves are absorbed to avoid reflection. The reactor is placed vertically within the transmission duct, sealed with rubber O-ring and stainless-steel sealers. The reactor is purged with a constant flow (1.5 L/min) of high purity nitrogen (N_2) gas (supplied by Praxair Canada Inc.) before, during, and after the reaction to ensure an oxygen-free environment. An infrared (IR) sensor (supplied by Hoskin Scientific Ltd., Burnaby, Canada) is installed above the reactor to measure the bed top surface temperature. The IR sensor is cooled with water for the duration of the reaction to prevent over-heating. The sensor is also purged by a buffer of N_2 gas to prevent vapour condensation.

During reaction, N_2 carries the pyrolysis vapours upward through the reactor toward the IR sensor. The vapours are diverted from the sensor via the second N_2 buffer gas. They flow through a line heated with electrical tape (to prevent vapour condensation) toward a two-stage condenser tube system. The condenser tubes are cooled counter-currently with cooling water. Any condensates (bio-oil) are condensed in a round-bottom collection flask. The non-condensable gases are purged with the N_2.

The set-up is depicted in Figure 8 and Figure 9.

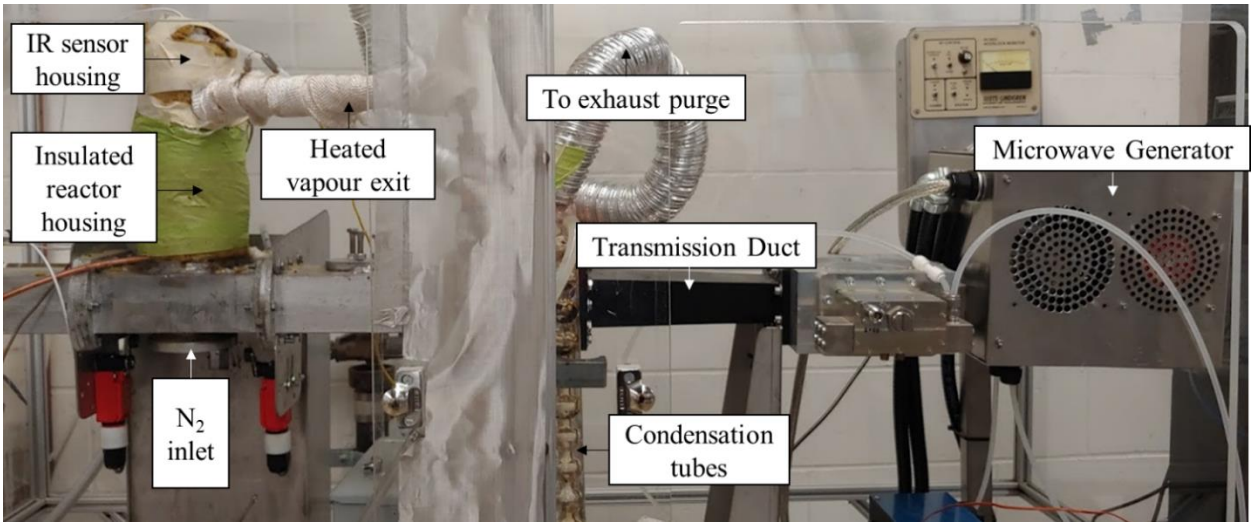

Figure 8: Labelled image of microwave pyrolysis set-up

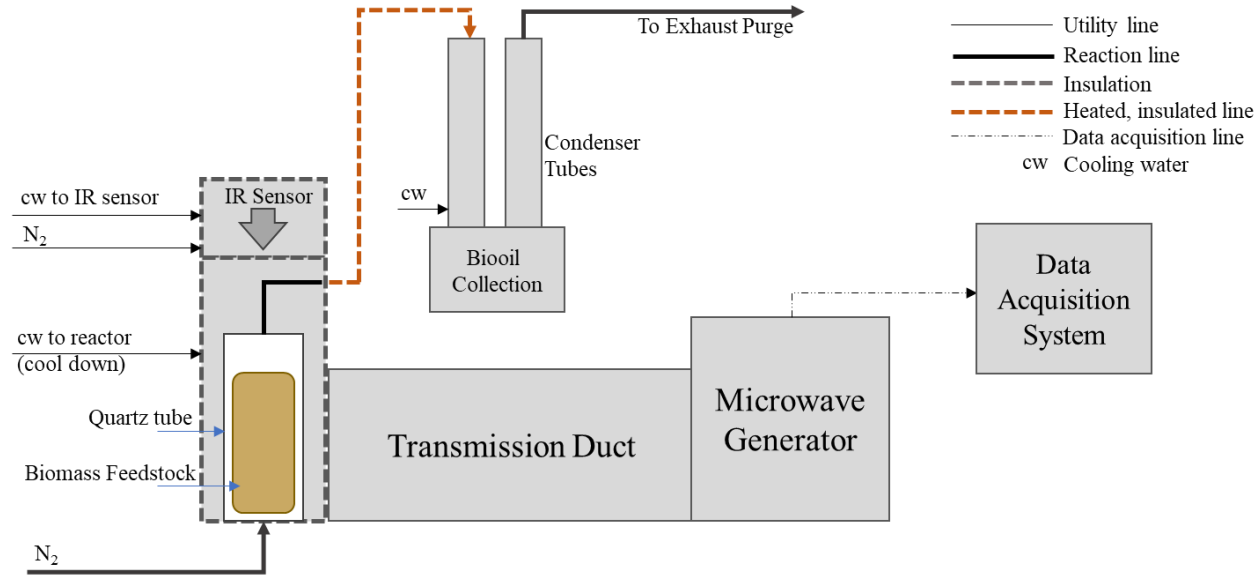

Figure 9: Schematic of microwave pyrolysis set-up

3.3 Experimental Design

3.3.1 Task 1: Determine Pyrolysis Conditions to Produce Graphitic Coke

10 g sawdust + 30 wt% K_3PO_4 is mixed and layered with 150 wt % SiC particles, in about 10 layers. The sawdust feedstock is always at the top layer to ensure more accurate IR sensor

temperature readings. The feedstock is heated at full microwave power (1200 W) until the desired reaction temperatures of 350, 450, and 550 °C are reached, at which time the microwave power is manually adjusted to maintain the temperature for 30 min or 50 min. The effect of heating rate will not be studied as it is difficult to control manually. However, it is expected that the time on stream (TOS) will have a similar effect; slow heating rates are suggested to allow sufficient time for oxygen-functional group to crack, a circumstance that could be mimicked from increased reaction times [55].

The reacted biochar + coked K_3PO_4 + SiC mixture is separated using a 2 mm and 150 µm sieve. The SiC pellets are > 2 mm and are collected to be washed, burned (using a muffle furnace at 600 °C for 24 h), and reused. Particles <150 µm are classified as coked K_3PO_4. Particles >150 µm but < 2 mm are classified as biochar. An image of the samples before and after separation is shown below (Figure 10). The coked catalyst sample is then analyzed using Raman spectroscopy, thermogravimetric analysis/derivative thermogravimetric analysis (TGA/DTG), elemental analysis (EA), scanning electron microscopy (SEM), and a dielectric probe kit.

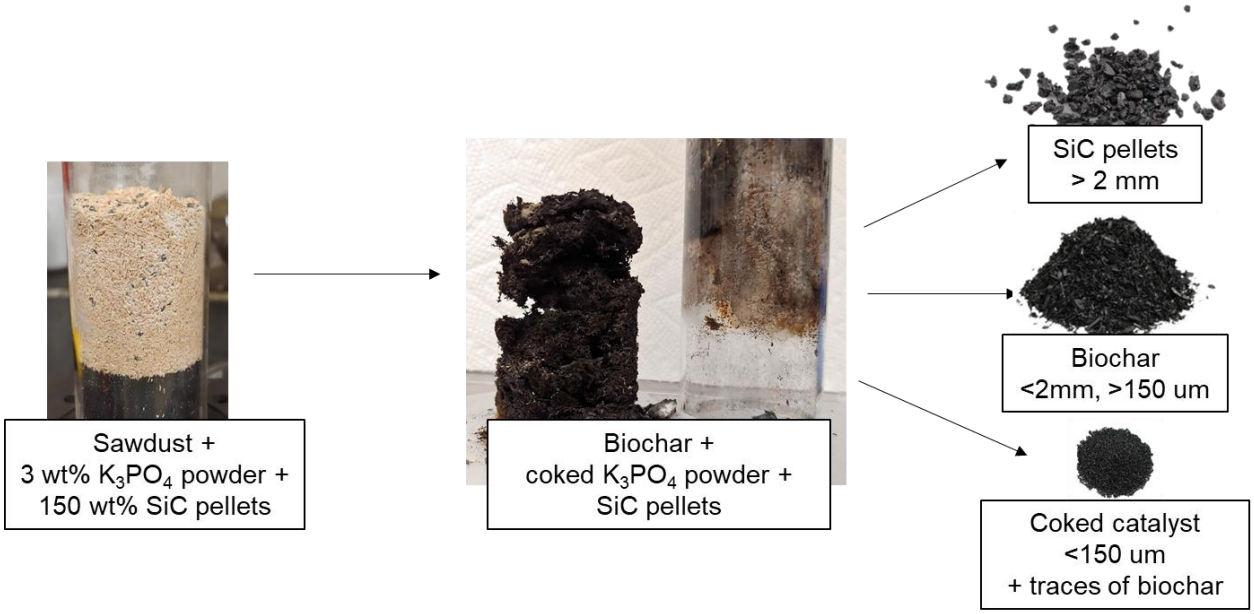

Figure 10: Conversion of sawdust into biochar and extraction of coked catalyst from the biochar mixture.

Raman spectroscopy

The coked K_3PO_4 is characterized via Raman Spectroscopy at UBC's department of Materials Engineering. The samples were each pressed firmly between two quartz plates and placed under the laser using a 0.3 filter and 5s acquisition time. All measurements were taken in a dark room. The peak measurements were analyzed using the deconvolution method in OriginPro 2015.

TGA/DTG

The coke combustion temperature was measured using TGA/DTG at UBC's Department of Forestry. MiJung Cho in Dr. Scott Renneckar's group assisted in operating the TGA. About 5 mg of the sample were placed in a platinum pan. The balance gas was nitrogen at 40 mL/min. The sample gas was air at 60 mL/min. The sample was heated to

600 °C at a rate of 10 °C/min and then cooled back to room temperature. The DTG peaks were analyzed using the deconvolution method in OriginPro 2015.

Elemental Analysis

The coked K_3PO_4 were sent to Echonotech Laboratory Services in Delta, BC for EA. The samples were dried at 105 ± 3°C prior to analysis. The elemental composition was determined by automated flash combustion and gas chromatography.

SEM

Images of the coked K_3PO_4 were taken using a Philips XL-30 SEM at UBC's Department of Earth, Ocean, and Atmospheric Sciences.

Dielectric Factors

The dielectric properties of the sawdust, fresh and coked K_3PO_4, and SiC powder were measured using the N1501A Dielectric Probe Kit coupled with the ENA Series Network Analyzer from Keysight technologies. The samples were separately placed into a vial ensuring that the sample height was at least 2 cm. The dielectric coaxial probe was placed on the surface of the samples and pressed down until the sample was firm. The dielectric factors (Ɛ' and Ɛ") were then measured using the probe. Since the sawdust was a porous powder, some air pockets trapped in the solid particles likely interfered with the dielectric measurement. The following formula, called the Complex Refractive Index mixture equation (CRIME) was use to extract the dielectric factors of the sawdust particles alone [70]:

$$\varepsilon^{\frac{1}{2}} = v_1(\varepsilon_1)^{\frac{1}{2}} + v_2(\varepsilon_2)^{\frac{1}{2}}$$

$$\varepsilon = \varepsilon' - j\varepsilon'' \text{ where } j = \sqrt{-1}$$

in this case, v and ε are the volume fraction and the complex relative permittivity, and the subscripts *1* and *2* represent the air and solid sawdust components. For air, the complex permittivity (ε_1) is $1 - 0j$ [70].

3.3.2 Task 2: Understand the Microwave Absorbance Properties of Coke

Three samples are separately tested for microwave absorbance: (1) sawdust, (2) 10 g sawdust + 30 wt% fresh K_3PO_4 and (3) 10 g sawdust + 30 wt% coked K_3PO_4 (coked at 550 ˚C for 50 min). The samples with K_3PO_4 are well mixed before being added into the reactor. The microwave is set to a constant power of 1200 W for 30 min. The temperature is recorded over the duration of the reaction.

3.3.3 Task 3: Investigate Coke as a Slow-release Fertilizer Coating

Part 1: Coked K_3PO_4 Preparation

A greater fraction of K_3PO_4 is mixed into the feedstock for this set of experiments to ensure that enough coked K_3PO_4 can be separated post-reaction for the soil leaching tests. 10 g sawdust + 150 wt% K_3PO_4 (total mixture weight of 25 g) is well mixed and added into the reactor. No SiC is added to these columns as the weight fraction of K_3PO_4 is enough to reach targeted reaction temperatures under the microwave irradiation. The feedstock is heated at full microwave power (1200 W) until the desired reaction temperatures of 350 and 550 ºC are reached. Then, the microwave power is manually adjusted to maintain the temperature for 30 min or 50 min. To

recycle the coke, the entire biochar + coked K_3PO_4 mixture (from the 550 °C and 50 min run) is mixed with enough fresh sawdust to have a final feedstock weight of 25 g. This feedstock is heated at full microwave power to a desired reaction temperature of 550 ^oC, and the reaction is held at this temperature for 50 min. The biochar + coked K_3PO_4 mixtures are separated following procedures described previously. The coked K_3PO_4 is separated as particles < 150 µm.

Part 2: Potassium and Phosphate Leaching

Fresh (not dried) soil was used in all leaching experiments. The samples prepared for leaching include:

a. 50 g soil ("blank column")
b. 50 g soil + 2 wt% fresh K_3PO_4
c. 50 g soil + 2 wt% coked K_3PO_4 (coked at 350 °C and 30 min)
d. 50 g soil + 2 wt% coked K_3PO_4 (coked at 550 °C and 30 min)
e. 50 g soil + 2 wt% coked K_3PO_4 (coked at 550 °C and 50 min)
f. 50 g soil + 2 wt% recycled K_3PO_4 (coked twice at 550 °C and 50 min)

A fraction of 2 wt% fresh and coked K_3PO_4 was chosen based on methodology found in the literature which tested leaching of K^- and PO_4^{3+} from biochar [71]. All samples are prepared in duplicates. The samples are well mixed and loosely added into vertical columns made from 250 mL PVC syringes (Figure 11). The bottoms of the syringes are lined with 20 µm filter paper and 100 µm stainless steel mesh screens.

Figure 11: Soil and K_3PO_4 samples packed into PVC syringes

The leaching test was performed on a per-volume of water basis, rather than a per-time basis, for this preliminary experiment, since it was expected that the water would drain through the column quite quickly (in a range of minutes) and that the K_3PO_4 would leach easily [72]. The 50 g soil sample fills about 50 mL of the syringes, which can hold a volume of 20 mL water (defined as one pore volume PV). A pre-determined number of PVs of deionized (DI) water are added to the column every 45 min. The water leaches out of the column after about 5 min. 1 mL of water (leachate) is collected from a beaker at the bottom of each syringe and diluted in 5 mL of DI water for testing. After each collection, the leachate is emptied from the beaker before the next PV of DI water is added. It is important to know what fraction of the coked K_3PO_4 is K_3PO_4 in the samples being mixed with soil. To determine this, 1 g of the same samples being mixed with soil are added to 50 mL of DI water and stirred every hour for 6 h. It is assumed that 100 % of the K_3PO_4 is

leached out of the coke and into the water. 1 mL of this sample is collected through a syringe filter of 0.45 µm. The sample is diluted in 5 mL DI water for testing. The elemental concentrations of K and P are measured using inductively coupled plasma optical emission spectrometry (ICP-OES):

ICP-OES

The leachate was sent for ICP-OES testing at UBC's Department of Earth, Ocean, and Atmospheric Sciences with equipment model Varian 725ES. Each measurement was taken in triplicates under a run time of 3s. The method of analysis of ICP-OES results is shown in the appendix.

Chapter 4: Results and Discussion

4.1 Experimental Troubleshooting

4.1.1 Coked K_3PO_4 Collection

Researchers studying coking of solid catalysts often employ either liquid or gaseous hydrocarbons. This makes the solid catalyst easier to be separated post reaction as the liquid biooil or gaseous hydrocarbons can be condensed [46], filtered [44], or purged out [49], [73]. In this project where biomass particles decompose to hydrocarbons and subsequently cracked *in-situ*, difficulty arises in separating coked K_3PO_4 catalyst from the solid biochar. K_3PO_4 readily absorbs water and dissolves in water, and thus cannot be separated by washing or by a density segregation in water or other liquid. In the design of the experiment, the reactor was initially divided into two layers by a layer of quartz wool between a layer of sawdust + reaction K_3PO_4 mixture and a separate layer of pure K_3PO_4 for coking (Figure 12). During the reaction though, the glass wool became stiff and brittle and flaked in a fashion similar to the biochar, making it difficult then to separate the wool clearly from the coked K_3PO_4.

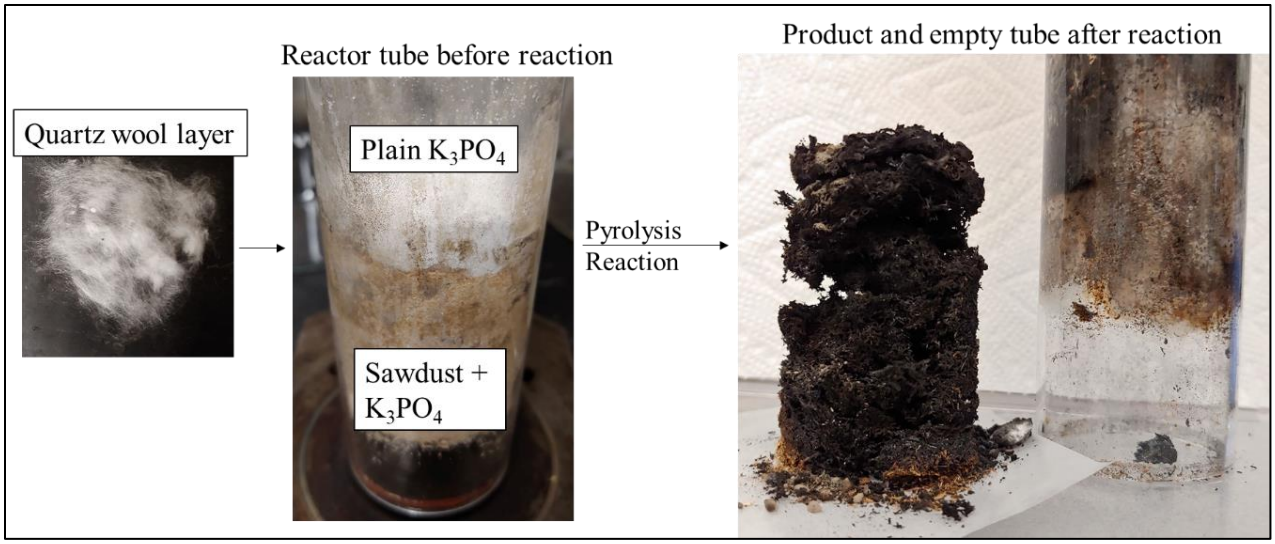

Figure 12: Quartz wool separation of K_3PO_4

Instead, for all of the following experiments, biochar was separated from the K_3PO_4 by size segregation, a method proposed and executed previously in our group [68]. The mixture of particles <150 μm was classified as coked K_3PO_4 (with traces of biochar). This method proved challenging as well. As K_3PO_4 absorbed water rapidly, sticking to the biochar particles and often clogging the sieve during separation, only about 20 wt% of the K_3PO_4 was recovered by this method.

4.1.2 Power vs Temperature

The temperature of reaction is controlled by manually adjusting the microwave power once the desired temperature is reached. Figure 13 shows the Temperature vs Time graph for three pyrolysis test runs where the temperatures were maintained at 350 ^oC, 450 ^oC, and 550 ^oC, each for 30 min. The feedstock for each reaction shown was 10 g sawdust + 30 wt% K_3PO_4. In each case, little biooil (in the order of droplets) was produced due to the vapour cracking reactions

catalyzed by K and P [20], [26]–[30]. The biochar yield was always around 30 wt%, with the remaining product yield (approximately 70 wt%) as gas products.

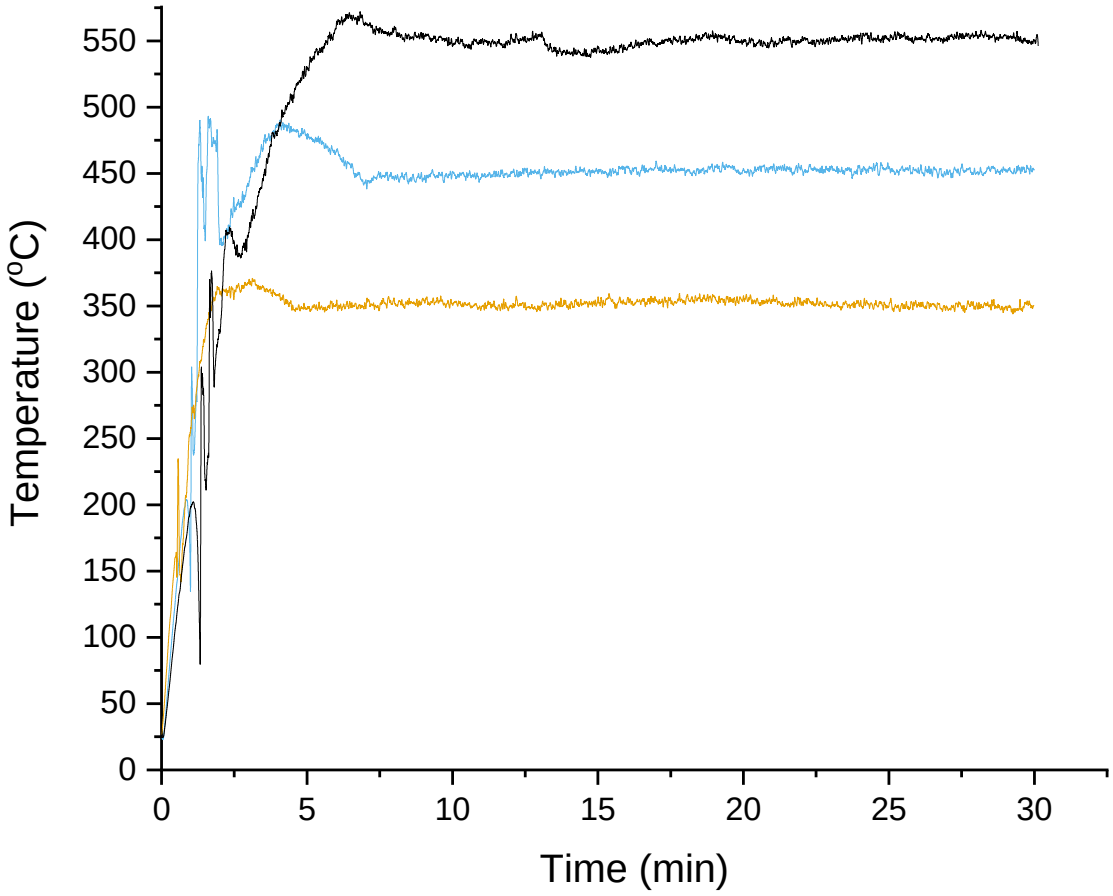

Figure 13: Recorded pyrolysis temperatures over three 30 min runs at: 350 °C (orange), 450 °C (blue), and 550 °C (black)

The initial heating rate was ~2.5 °C/s over the first 2.7 min of reaction before approaching reaction temperatures of 350 and 450 °C. For the test operated at 550 °C, the heating rate after 2.7 min decreased to about 0.5 °C/s until reaching the target temperature. These are heating rates typical for slow pyrolysis [14], [20]. Because the temperature was measured from the bed top (via IR sensor) and the temperature was controlled by manually adjusting the power, some fluctuations in the temperature-power relationships were observed, shown by the large error bars in Figure 14 (i.e. to maintain a temperature of 450 °C, the required power could range between 250 – 600 W).

This is likely due to the heterogeneity of the sample caused from differences in particle size among the K_3PO_4 (fine powder), sawdust particles (300 – 600 µm), and SiC granules (2 mm). This size distribution is designed to enable the recovery of K_3PO_4 for analysis and SiC pellets for reuse. However, it also causes inconsistencies in mixing and distribution. The effect of the mixing inconsistency is amplified when temperature is recorded with the IR sensor, as it can only measure the top surface temperature of the sample, which is likely not an accurate representation of the entire sample.

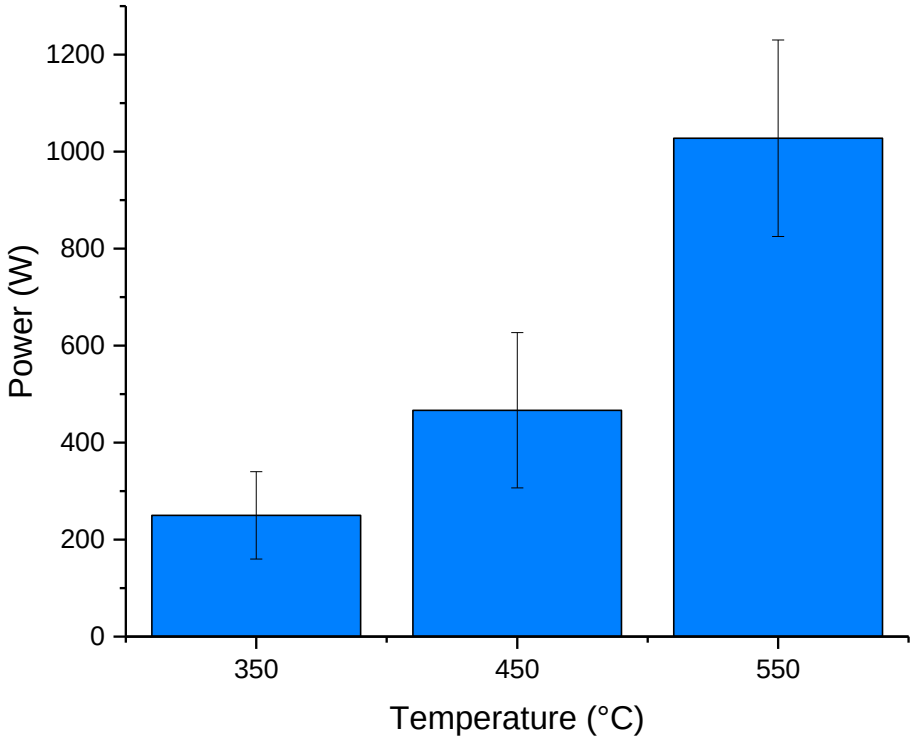

Figure 14: Average microwave power settings to reach selected temperatures

4.2 Coke Characterization

4.2.1 Graphitic-to-Oxygenated Coke Ratio

Raman spectroscopy is a common technique to characterize the carbon bonding of coked catalysts [44], [47], [49]. Bond types are labelled based on the band position from the Raman shifts. Carbon bond labels are given in Table 11 from [68].

Table 11: Raman shift band positions typical for carbon-based species [68]

Band Name	Band Position (cm^{-1})	Description	Bond Type
GL	1700	carbonyl group C=O	sp^2
G	1590	Graphite, aromatic ring quadrant breathing, alkene C=C	sp^2
GR	1540	aromatics with 3–5 rings, amorphous carbon structures	sp^2
VL	1465	methylene or methyl, semicircle breathing of aromatic rings, amorphous carbon structures	sp^2, sp^3
D	1340	D band on highly disordered carbonaceous materials, C-C between aromatic rings and aromatics with no less than six rings	sp^3
SL	1230	aryl−alkyl ether, para-aromatics	sp^2, sp^3
S	1185	$C_{aromatic}$−C_{alkyl}, aromatic (aliphatic) ethers, C-C on hydroaromatic rings, hexagonal diamond carbon sp^3, C-H on b aromatic rings	sp^2, sp^3
SR	1060	C-H on aromatic rings, benzene (ortho-disubstituted) ring	sp^2
R	960-800	C-C on alkanes and cyclic alkanes, C-H on aromatic rings	sp^2, sp^3

The band shifts of coked K_3PO_4 were compared to those of pure graphite powder as a reference. The graphite powder showed clear D- and G-peaks, whereas the coked K_3PO_4 (regardless of preparation temperature) displayed peaks with much lower intensity (350 °C coked K_3PO_4 is shown in Figure 15).

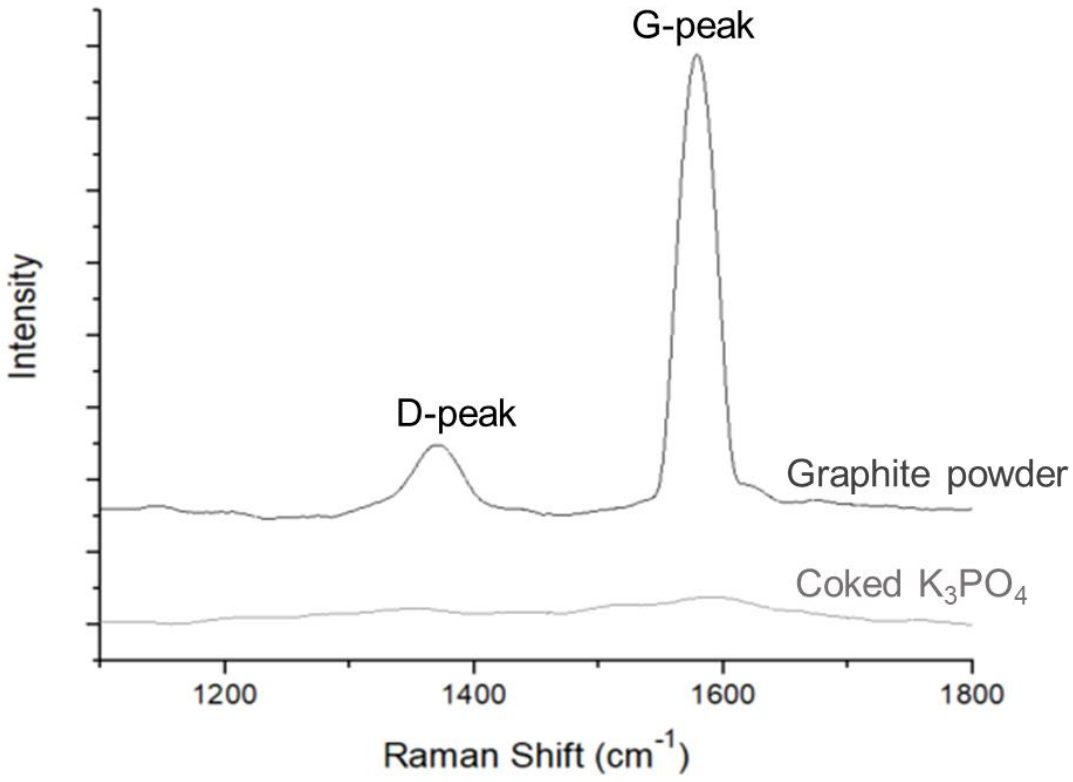

Figure 15: Raman shift of graphite powder and 350 °C coked K_3PO_4

Over a smaller intensity range the coked K_3PO_4 samples shows slight D- and G-peaks. The Raman Shift of 350 °C coked K_3PO_4 is shown in Figure 16a. However, the repeatability is quite low, causing large error bars in the G:D ratio analysis (Figure 16b). It was expected that the G:D ratio would increase as the pyrolysis (coking) temperature increased, as suggested by the fact that the carbon becomes more graphitic as oxygen bonds are cleaved off at higher temperatures. The

Raman Shifts, however, were inconclusive. This is likely because the fraction of carbon in the sample is mixed with the K_3PO_4, causing sample heterogeneity and the fraction of carbon too low to be detected.

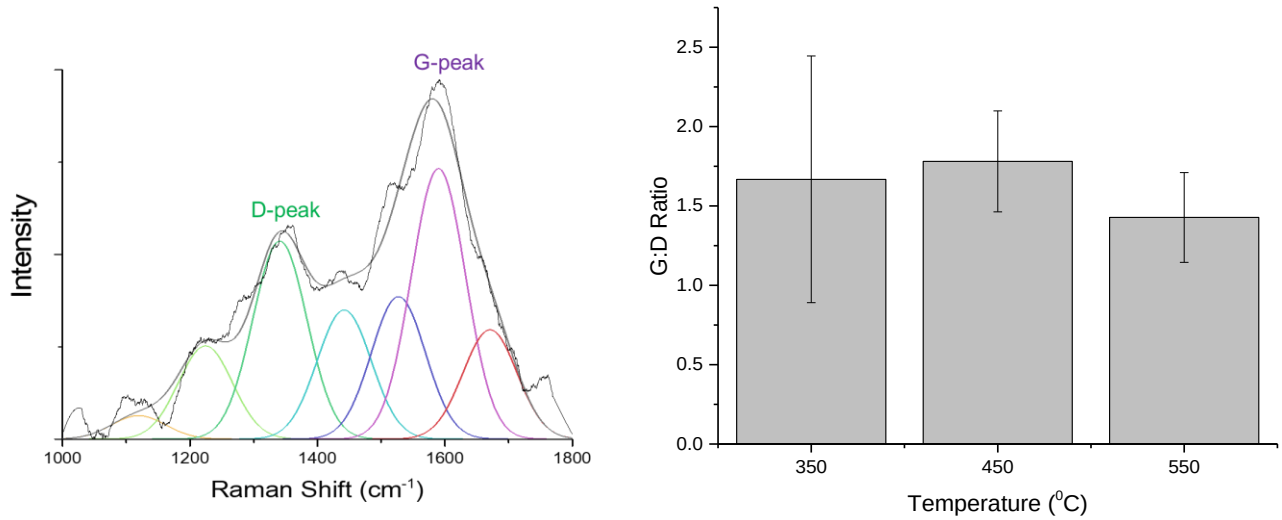

Figure 16: (a) Raman shift of 350 ºC coked K3PO4 and (b) G:D ratio of coked K_3PO_4 at increasing pyrolysis (coking) temperature

Another method of characterizing coke type is through its combustion temperature. Combustion DTG curves of coked catalyst are shown in Figure 17 between 200 – 600 ºC. It has been reported that coke combustion begins between 200 – 230 ºC, and displays two distinct decomposition peaks. The first peak occurs between 200 – 350 ºC, representing the combustion of oxygenated coke. The second occurs between 350 – 600 ºC, representing the combustion of graphitic coke [53], [68], [73]. The peak area representing oxygenated coke decreases as the coking temperature increased from 350 °C to 550 °C and even more so when the coking time increased from 30 min to 50 min. Indeed, this result is exactly what was expected: the oxygen functional groups are cleaved off as the coking temperature and reaction time are increased. The peak areas representing graphitic coke, however, follow a less clear trend with coking conditions.

Nevertheless, the ratio of graphitic to oxygenated peak areas shows a clear increase with increasing coking temperature and reaction time. It should also be noted that the peak region representing graphitic coke (350 – 600 °C) appears to contain 2 peaks within itself, one between 350 – 440 °C and another at 440 – 600 °C, implying that the graphitic coke compound may in fact be broken down into two separate compounds which burn under slightly different temperature conditions. The same result was found in another study, but the actual difference in compound structure remains unknown [73].

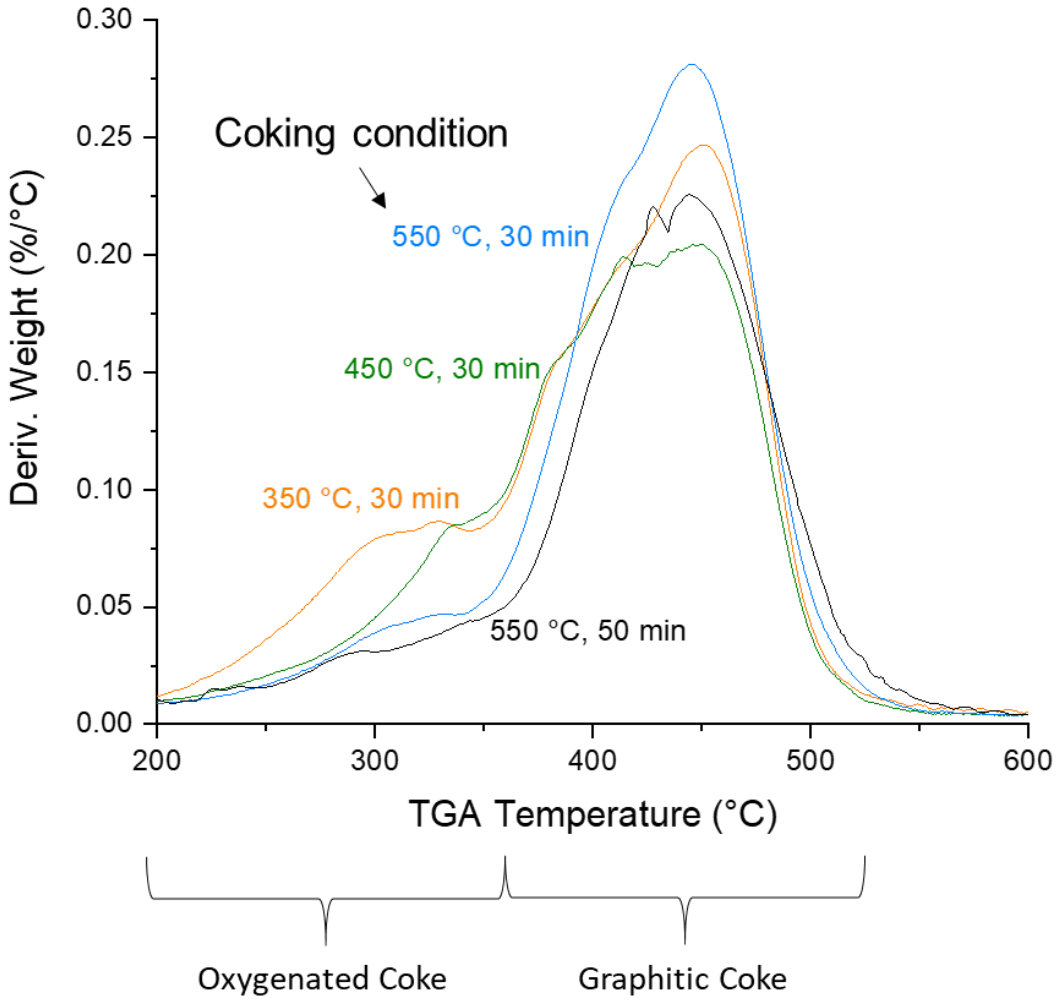

Figure 17: Combustion DTG curves of coked K_3PO_4 at different coking conditions

Using the deconvolution method, the peak areas of both coke types were estimated to generate a ratio of graphitic-to-oxygenated coke at each pyrolysis temperature (Figure 18). The ratio of graphitic-to-oxygenated coke (G:O) increases linearly with increasing pyrolysis temperature between 350-550 ^{o}C, meaning that that the coke type can be successfully controlled based on reaction temperature.

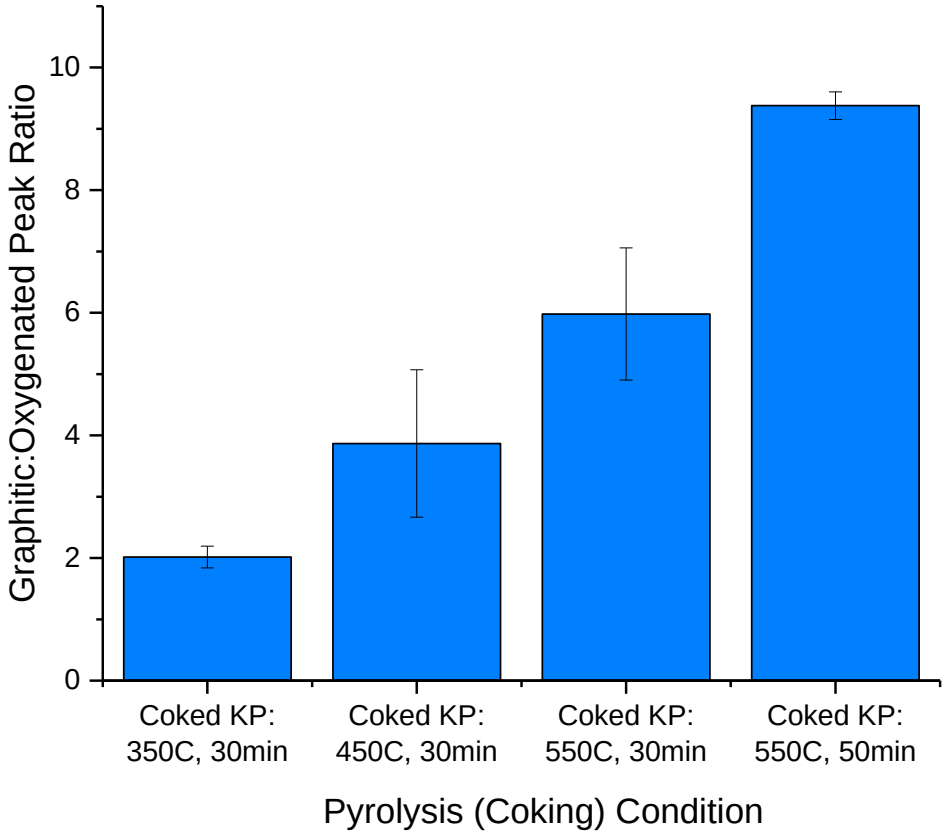

Figure 18: Ratio of graphitic to oxygenated peak areas of coked K_3PO_4 at different coking conditions, derived from DTG data

4.2.2 Coke Yield

TGA can be used to estimate the actual amount of coke deposited on the catalyst. Some mass losses occurred between 25 – 200 °C but were classified as either water, low temperature volatiles

or trace-catalyst losses [73]. All coke started to burn pronouncedly only above 200 °C, and seen to be completely combusted by 600 °C. The coke yield (%) was taken as total weight % combusted between 200 – 600 ºC and is shown in Figure 19. The data suggest that lower pyrolysis temperatures and longer reaction times produce a slightly greater amount of coke, although all were around 40 wt% (41, 38, and 37 wt% for 350, 450, and 550 °C pyrolysis temperatures and 39 wt% for 550 °C at 50 min). This is consistent with reported results which suggest that high temperatures promote the decomposition of coke [49].

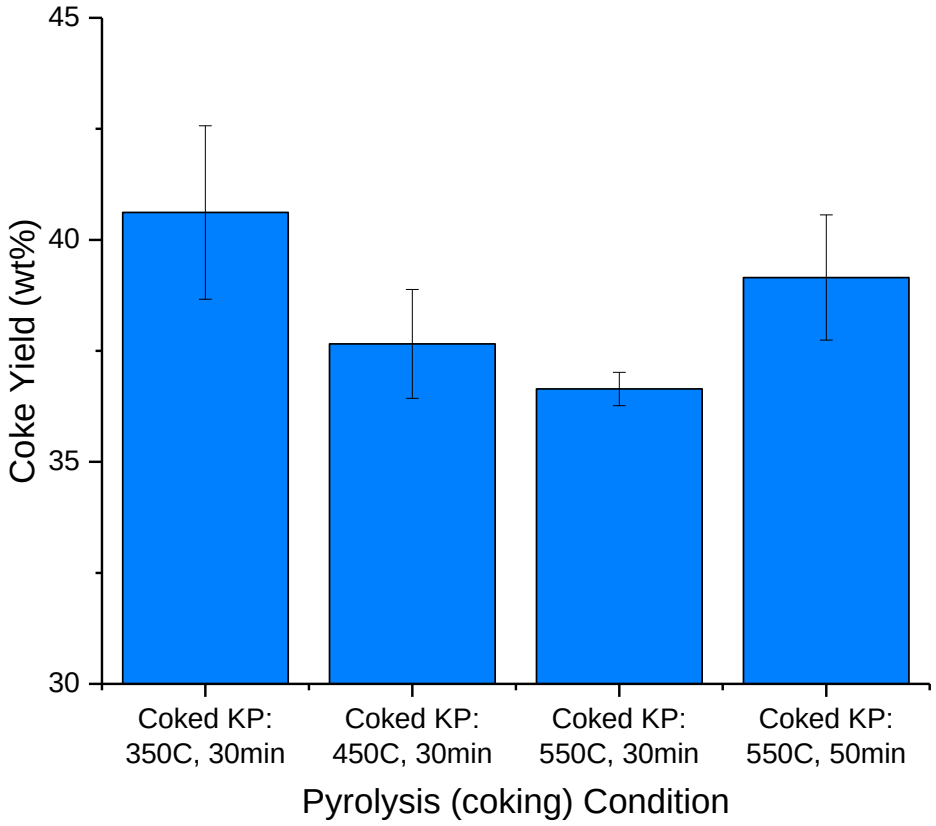

Figure 19: Coke yield of coked K_3PO_4 at different coking conditions, derived from TGA data between 200 – 600 ºC

Elemental analysis (C, H, N, O) of coked K_3PO_4 was also performed to observe elemental changes over coking conditions (Figure 20). Nitrogen was not detected in any sample. The change

in oxygen could not be accurately analyzed as it included oxygen from both coke and K_3PO_4, with the fraction of each being unknown. The fractional change in carbon between each coking condition is well correlated to the change in coke yield (Figure 19). The percentage of carbon in the coked K_3PO_4 sample decreases as the total fraction of coke (yield of coke) within the sample decreases, corresponding to the increase in the reaction temperature at a fixed reaction time. The percentage of carbon in the sample increased as the reaction time was increased, again, directly correlated with the increase in the total fraction of coke in the sample.

For hydrogen, there was no significant change among coked K_3PO_4 samples produced at different temperatures for 30 min, but there was a clear drop in hydrogen content between the 30 min and 50 min samples. This indicates that the longer reaction time promoted the cleaving of -OH and C-H groups and the formation of alkene C=C bonds. Similarly, the C/H ratio did not vary significantly between samples produced under 30 min, but there is a clear increase in the C/H ratio under the 50 min sample, also implying the promoted loss of oxygen functional groups under longer reaction times.

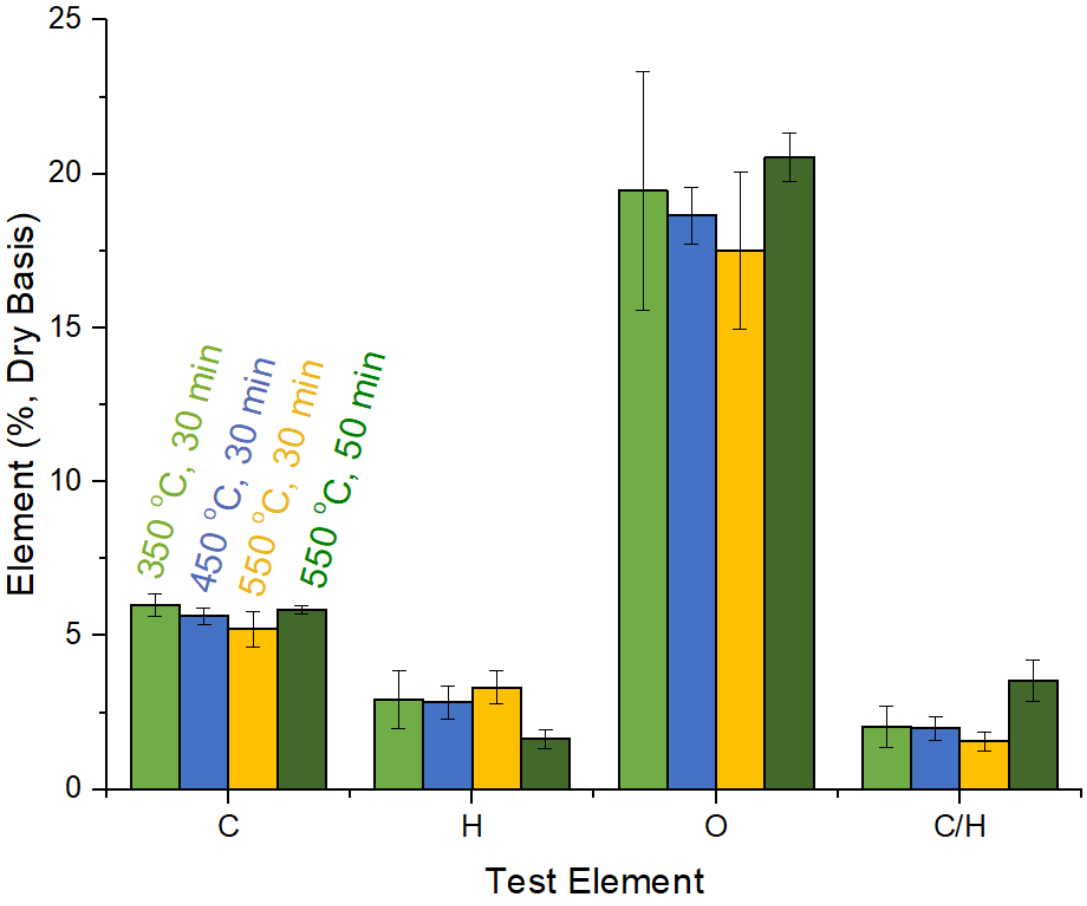

Figure 20: Elemental compositions of coked K_3PO_4 at different coking conditions

4.2.3 Coke Image Analysis

During pyrolysis, the K_3PO_4 catalyst turns from white to black, indicating that there is coke deposited on its surface (Figure 21).

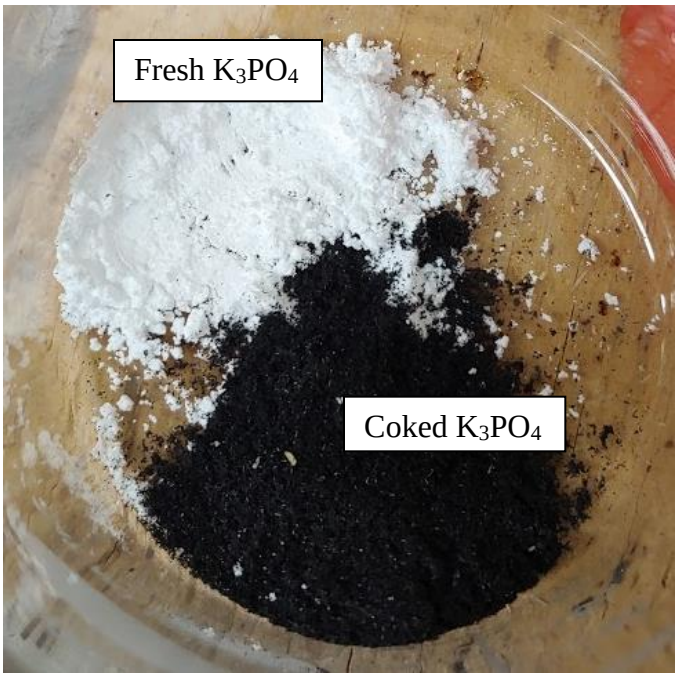

Figure 21: Colour change of fresh and coked K_3PO_4

The coke can be seen at a microscopic level using SEM imaging. Coked K_3PO_4 samples are shown in Figure 22. The fresh K_3PO_4, unfortunately, can not be imaged for comparison as it absorbs water from air so rapidly that it becomes a liquid under the microscope. Figure 22 shows spherical particles ranging from 1 – 20 μm. These particles have been attributed to coke formation, resulting from secondary gas-phase volatile reactions, similar to the spherical char nanoparticles from pyrolyzed woody biomass [47], [53], [74]. Similar spherical particles have been characterized as lignin nanospheres, or as aromatic 'clusters', forming from carbonization and polymerization of intermediate vapours [75], [76]. The overall mechanism of polymerized aromatics around a nucleus site is the same, whether it forms lignin nanospheres or coke spheres.

It was expected that higher pyrolysis temperatures would promote the accumulation of these particles [53], however, no clear difference is seen between samples prepared at different pyrolysis temperatures, likely because each sample contains a mixture of both oxygenated and graphitic

coke. Some trace amounts of biochar were seen in the coked K_3PO_4 samples (Figure 23), also with coke particles on their surface.

The same coked K_3PO_4 samples were also washed to remove K_3PO_4, which dissolved readily in water. The remaining coke and traces of fine biochar were dried and viewed under SEM as well. This time, the coke spheres had collapsed, or burst (Figure 24). This suggests that the spheres are hollow and easily break during washing with water.

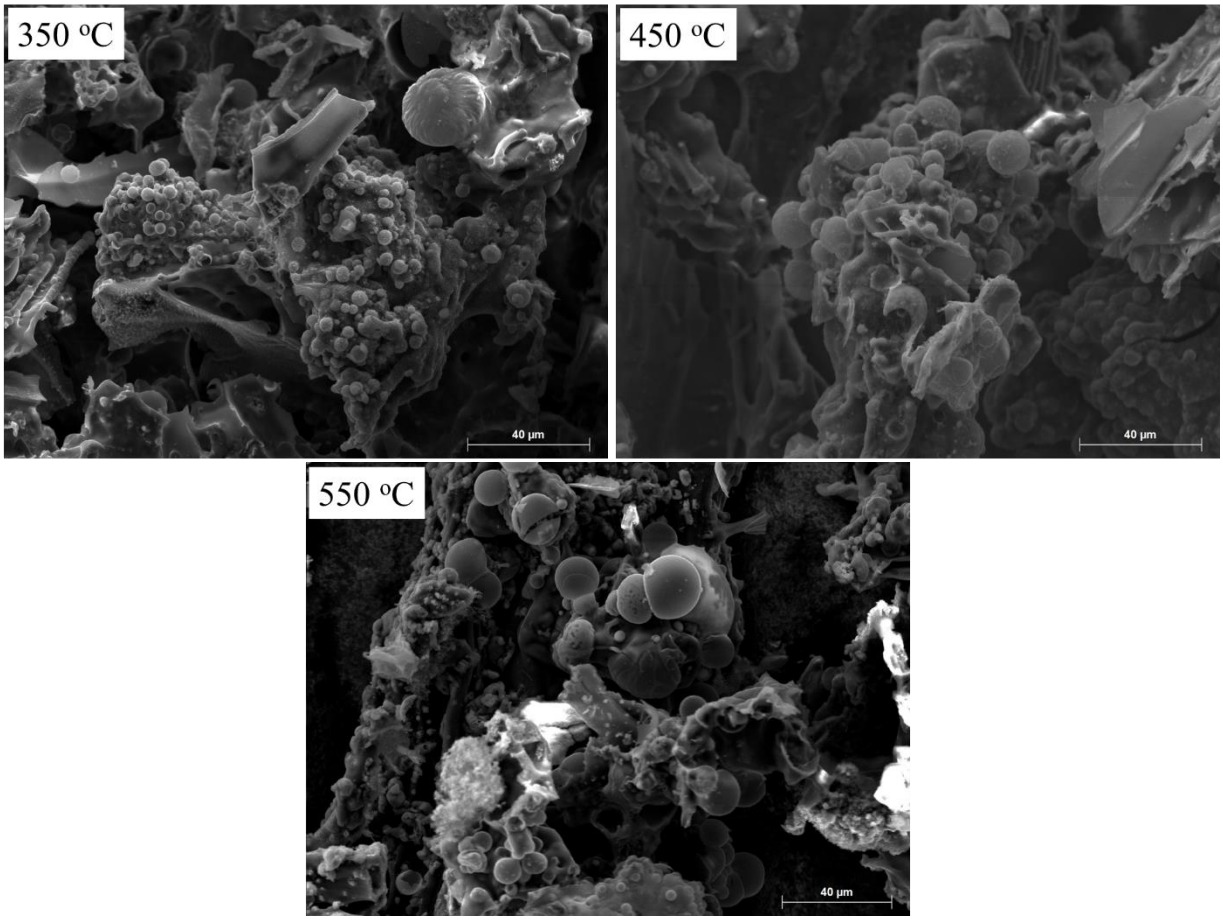

Figure 22: SEM of coked K_3PO_4 at different coking temperatures

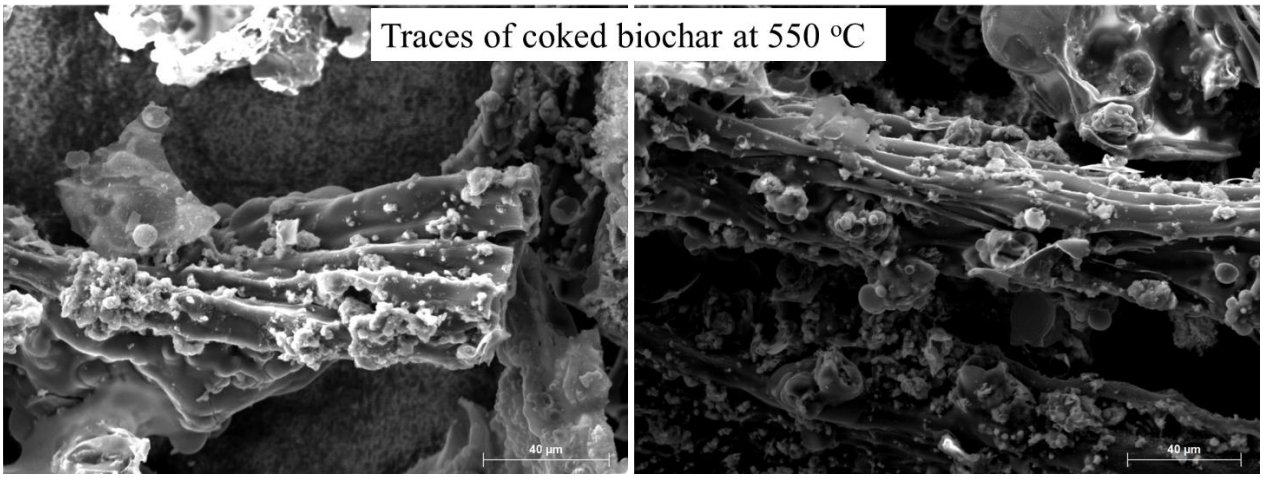

Figure 23: SEM of coked K_3PO_4 showing traces of coked biochar

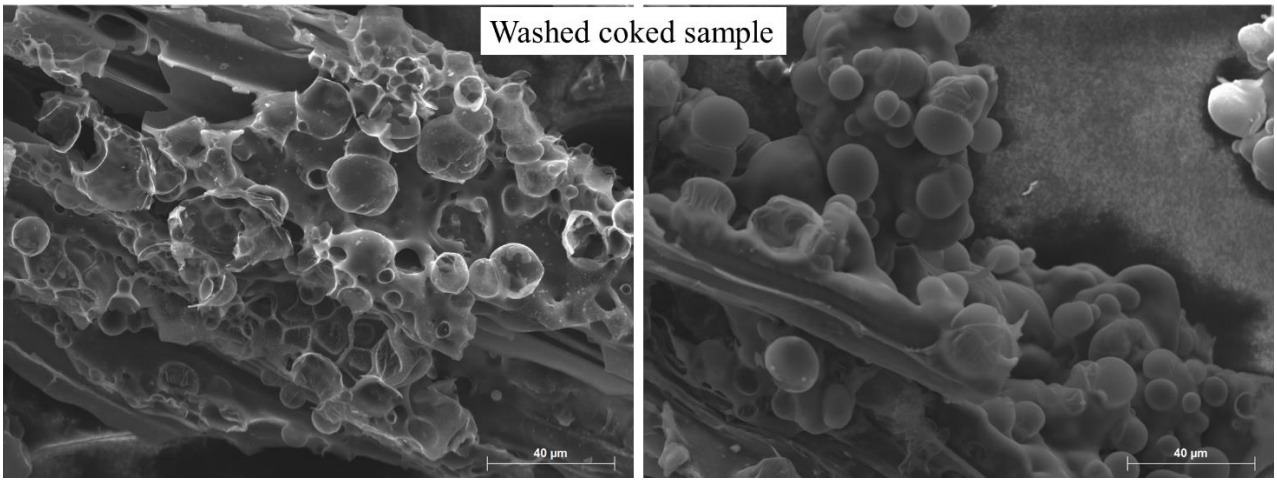

Figure 24: SEM of washed coked K_3PO_4

4.2.4 Summary of Coke Characterization

Based on the combustion characteristics of oxygenated and graphitic coke, DTG data suggests that the G:O ratio increases with increased preparation temperature and reaction time. Coke produced at 550 °C for 30 min has a 196 % increase in G:O ratio than that produced at 350 °C for the same reaction time. Subsequently, coke produced at 550 °C for 50 min has an even greater G:O ratio, 57 % greater than that produced at the same temperature for only 30 min. This trend is also reflected in the hydrogen content in the samples from elemental analysis; coke produced at a

longer reaction time contains less hydrogen, suggesting that dehydrogenation reactions have occurred, promoting the formation of graphitic coke.

If all coke burns between 200 – 600 °C [53], [68], [73], the coke mass loss from TGA data suggests that the coke yield on a coked K_3PO_4 sample decreases with increasing pyrolysis reaction temperature, but increases with increasing pyrolysis reaction time, although all coke yields remain around 40 wt%. This same trend is seen in the carbon content of the coked K_3PO_4 sample shown from elemental analysis.

Microscopic images show the coke as spherical bubbles on the surface of the K_3PO_4 and biochar traces. There is no noticeable difference in the amount or size of these spheres as the coking conditions change, likely because all samples contain both oxygenated and graphitic coke. The coke spherical structures are destroyed after the coked K_3PO_4 sample is washed through agitation in water and filtration.

4.3 Microwave Absorbance of Coked K_3PO_4

4.3.1 Dielectric Properties

The dielectric loss (Ɛ”, ability to release energy as heat) and dielectric constant (Ɛ’, ability to store microwave energy) were measured for fresh sawdust, SiC powder, fresh K_3PO_4, and coked K_3PO_4 at various coking conditions. Both dielectric factors of coked K_3PO_4 were greater than those of fresh K_3PO_4 and increased further with increasing coking temperature and reaction time. This is likely because higher temperatures and longer reaction times increase the G:O ratio of the coke, and the more graphitic (polyaromatic) the coke, the more pi-bonds are in its structure. This

promotes the Maxwell-Wagner-Sillar effect and subsequently a greater microwave absorbance [35].

Perhaps even more informative is the loss tangent shown in Figure 26. The loss tangent represents the ratio of Ɛ" and Ɛ', or, the ability to convert the absorbed electromagnetic energy into heat. The loss tangents of fresh K_3PO_4 and SiC are 300 and 1200 % greater than that of fresh sawdust. When added to the sawdust feedstock, they are proved to be good microwave absorbers.

The loss tangents of coked K_3PO_4 are even greater, being 1400 and 3000 % greater than fresh K_3PO_4 for coking conditions of 550 °C at 30 and 50 min, respectively. The loss tangent of the coke generated over 50 min is much greater than the 30 min coke because it not only has a greater G:O ratio, but also has a greater fraction of coke on the K_3PO_4 (coke yield, Figure 19). The loss tangent was expected to increase with increasing coking temperature, between 350 and 550 °C at 30 min, although it does not appear to differ greatly at these conditions. This could be attributed to the large error bars arising from the heterogeneity of the initial sawdust + K_3PO_4 powder feedstock, or to experimental errors in using the dielectric analyzer; the measurement will change as the force of the dielectric probe pressing down on the powder sample changes.

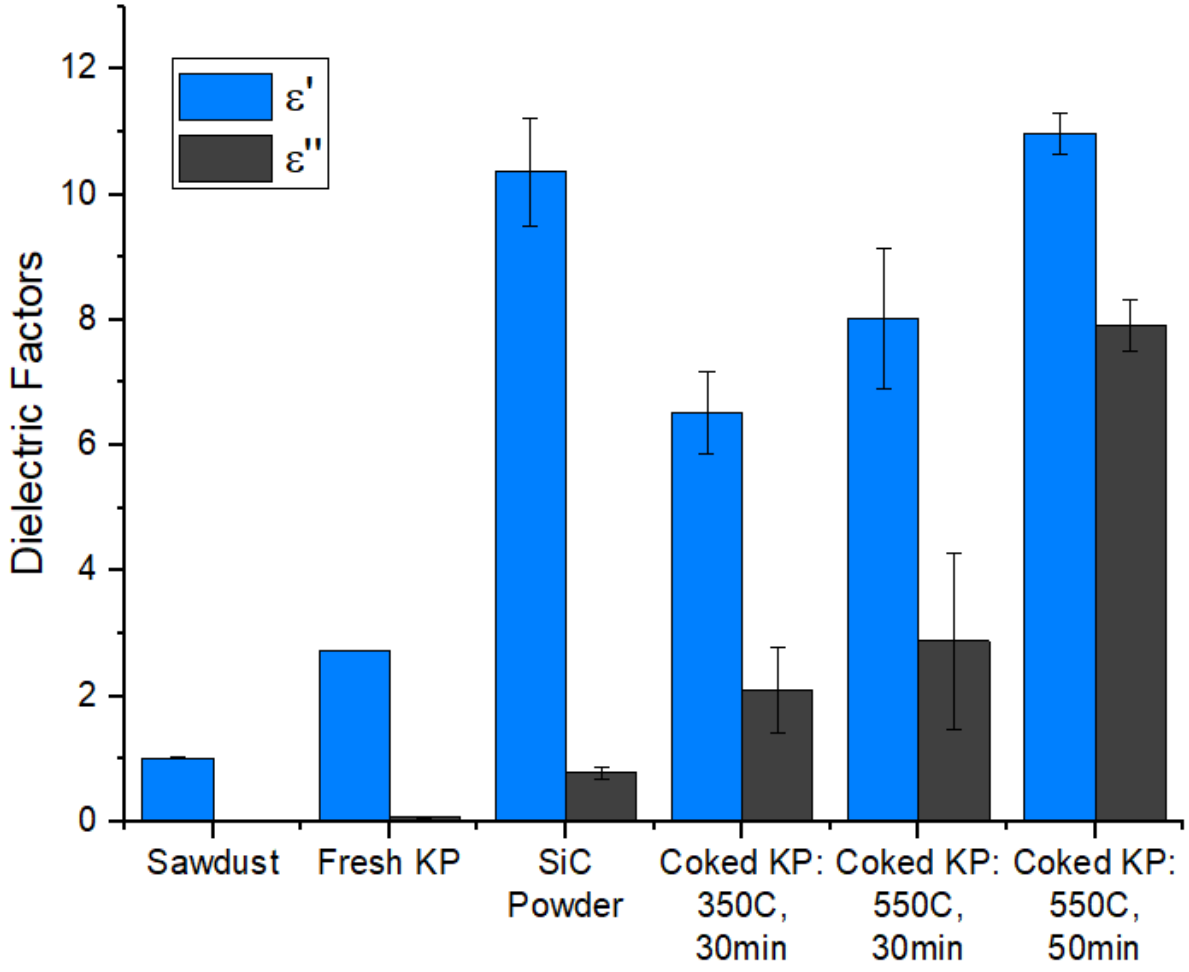

Figure 25: Dielectric loss (blue bars) and dielectric constant (black bars) of fresh sawdust, fresh K_3PO_4, and coked K_3PO_4 at various coking conditions.

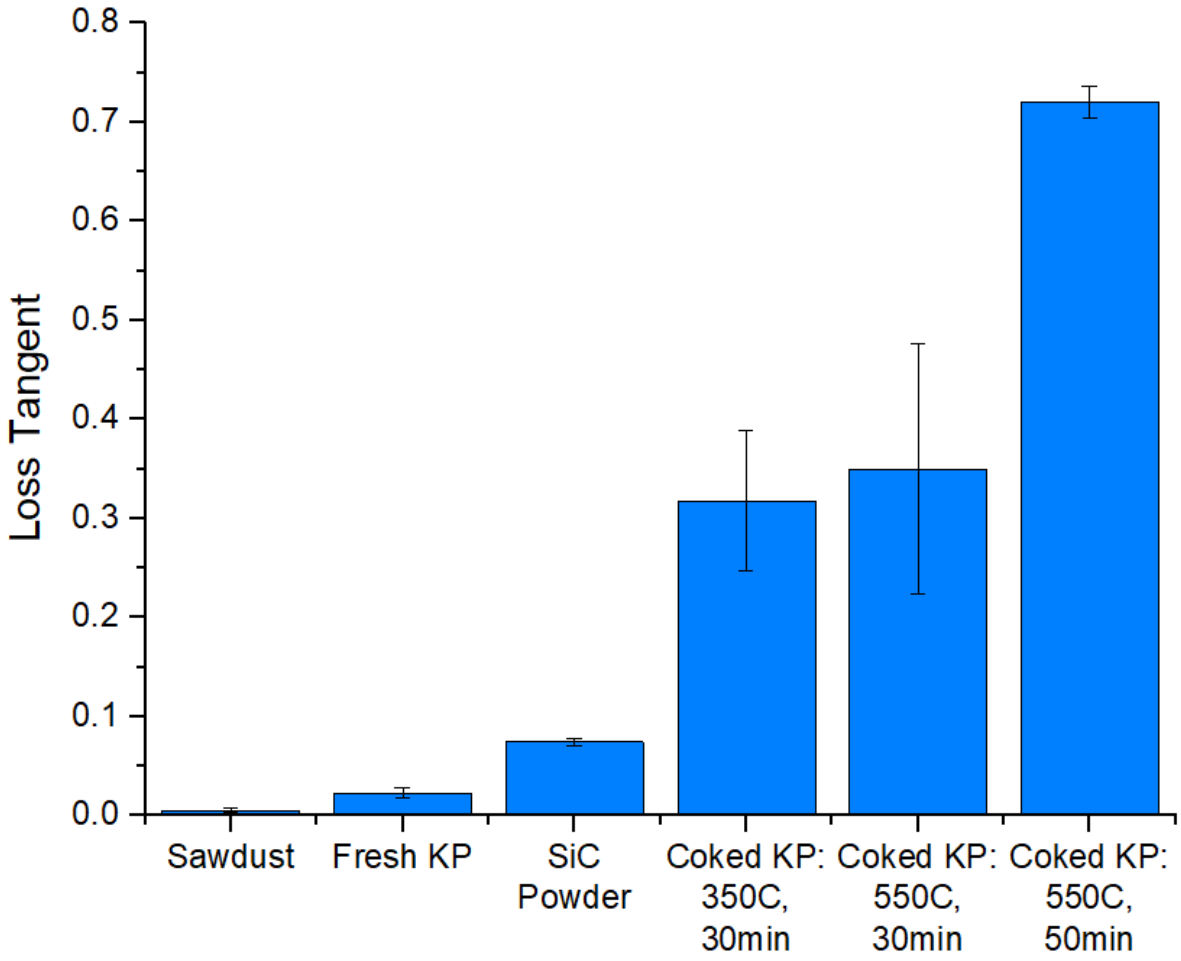

Figure 26: Loss tangent of fresh sawdust, fresh K_3PO_4, and coked K_3PO_4 at various coking conditions.

4.3.2 Reuse of Coked K_3PO_4

With the increased loss tangent of coked K_3PO_4 compared to fresh K_3PO_4, it was expected that the microwave absorption during pyrolysis would also be increased when the sawdust feedstock is mixed with spent (coked) K_3PO_4 rather than fresh K_3PO_4. The results are shown in Figure 27 for three different feedstocks: 1) plain sawdust, 2) sawdust mixed with 30 wt% fresh K_3PO_4, and 3) sawdust mixed with spent K_3PO_4 (previously coked at 550 $^{\circ}$C for 50 min). Each run was held at a constant power of 1200 W. Using the fresh and coked K_3PO_4 increased the steady-state pyrolysis temperature from 108 °C to 470 and 510 ^{o}C under the same microwave power,

respectively, suggesting that the coked K_3PO_4 indeed has a greater microwave absorption ability than the fresh K_3PO_4 during pyrolysis. However, the extent of this ability is lesser than was expected; the coked K_3PO_4 has a loss tangent 30 times greater than that of the fresh K_3PO_4, but it only improved the microwave absorption by 9 %. It is likely that its effects are diluted when only 30 wt% K_3PO_4 was added to the sawdust feedstock.

It is also important to note the noise in the temperature data collected over the spent K_3PO_4 (blue line in Figure 27). The spent (coked) K_3PO_4 produced more smoke during the reaction (likely from secondary cracking reactions) than the fresh K_3PO_4, causing interferences with the IR sensor and thus the noisy data.

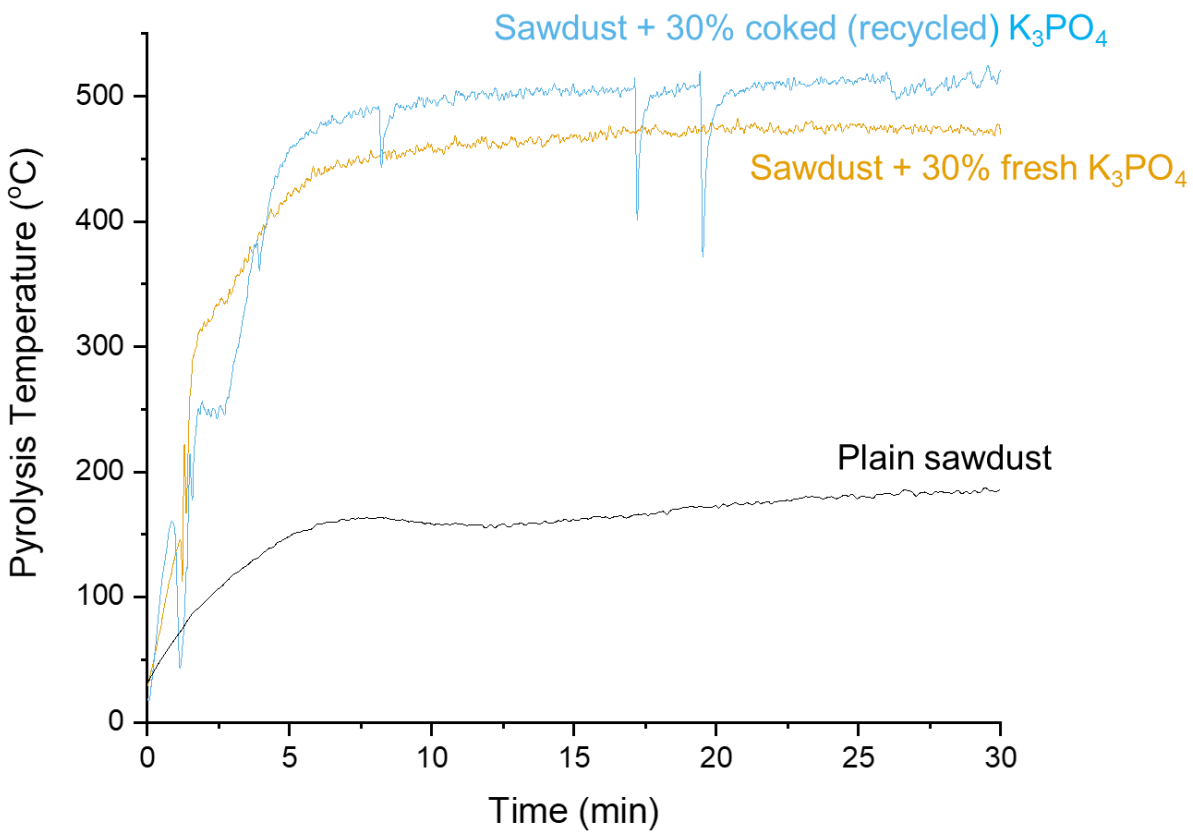

Figure 27: Pyrolysis temperature change with reaction time over a constant power of 1200 W for 1) plain sawdust, 2) sawdust with fresh K_3PO_4 , 3) and sawdust with spent (coked) K_3PO_4.

4.3.3 Summary of Coke Microwave Absorbance

The loss tangent of a substance represents its ability to convert electromagnetic energy into heat; the loss tangent of coked K_3PO_4 is greater than that of fresh K_3PO_4 by 30 times corresponding to the increased G:O ratio and coke yield. When recycling the coked K_3PO_4 at a 30 wt% loading in the sawdust, the spent catalyst increased the reaction temperature by 9 % compared to the same loading of fresh K_3PO_4. A greater K_3PO_4 loading would likely magnify this effect.

In the future work, it would be important to understand the change in catalytic activity between fresh and spent K_3PO_4. Typically, catalytic activity can be characterized by changes in

yield, acidity, water content and compositions of biooil. However, the fact that little biooil formed when either the fresh or coked catalyst was used does suggest that the K_3PO_4 is not deactivated after being used once [20], [26]–[30]. Another way to check catalytic activity is by analyzing the biochar, as K_3PO_4 has been reported to increase biochar BET surface area [32].

4.4 Coked K_3PO_4 as a Slow-Release Fertilizer

The soil set-up with leachate collection in shown below. The collected leachate appeared light yellow in colour for the blank (soil only) column, but a dark reddish-brown colour for all columns containing K_3PO_4 (Figure 28). The colour change must be from a reaction between the added K_3PO_4 and compounds in the soil. Note that the colour change could not be from the coke itself as: (a) the coke would have remained in the column above the 20 μm filter, and (b) the leachate from fresh K_3PO_4 (uncoked) also exhibited the colour change. As more PVs of DI water were added and collected from the soil, the colour became lighter yellow, suggesting that the K^+ and PO_4^- ions were washed out of the columns (Figure 29).

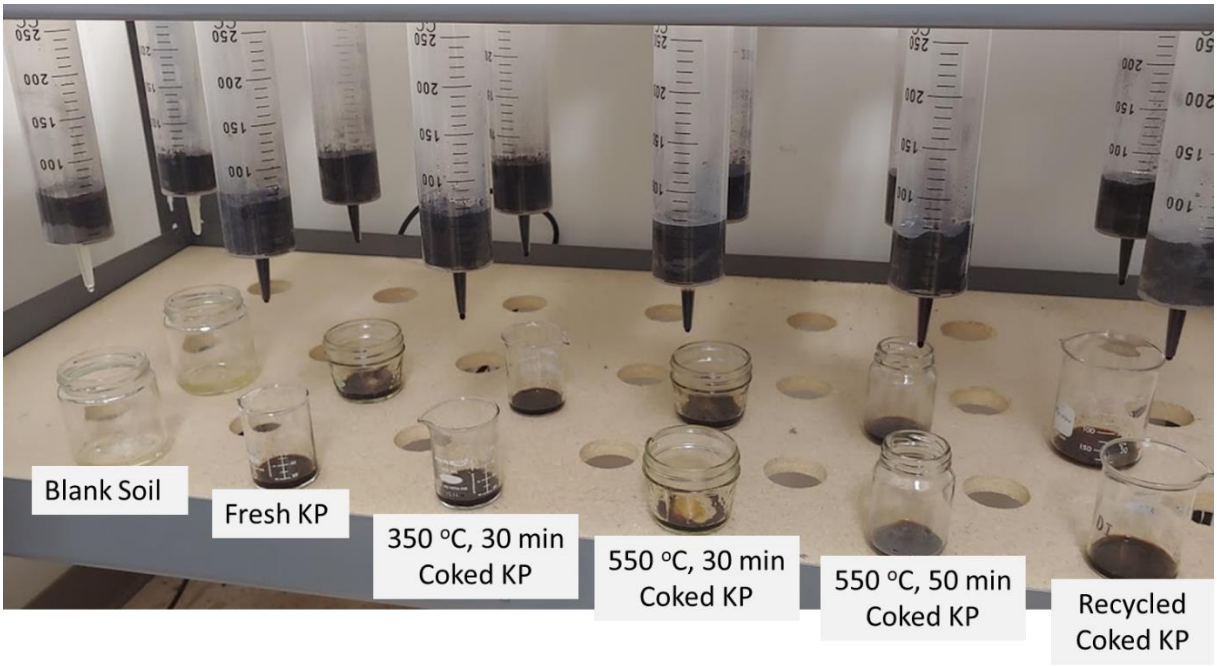

Figure 28: Leaching column set up, each condition in duplicates. Leachate is dark reddish-brown in colour for all columns of soil with 2 wt% fresh or coked K_3PO_4 (KP).

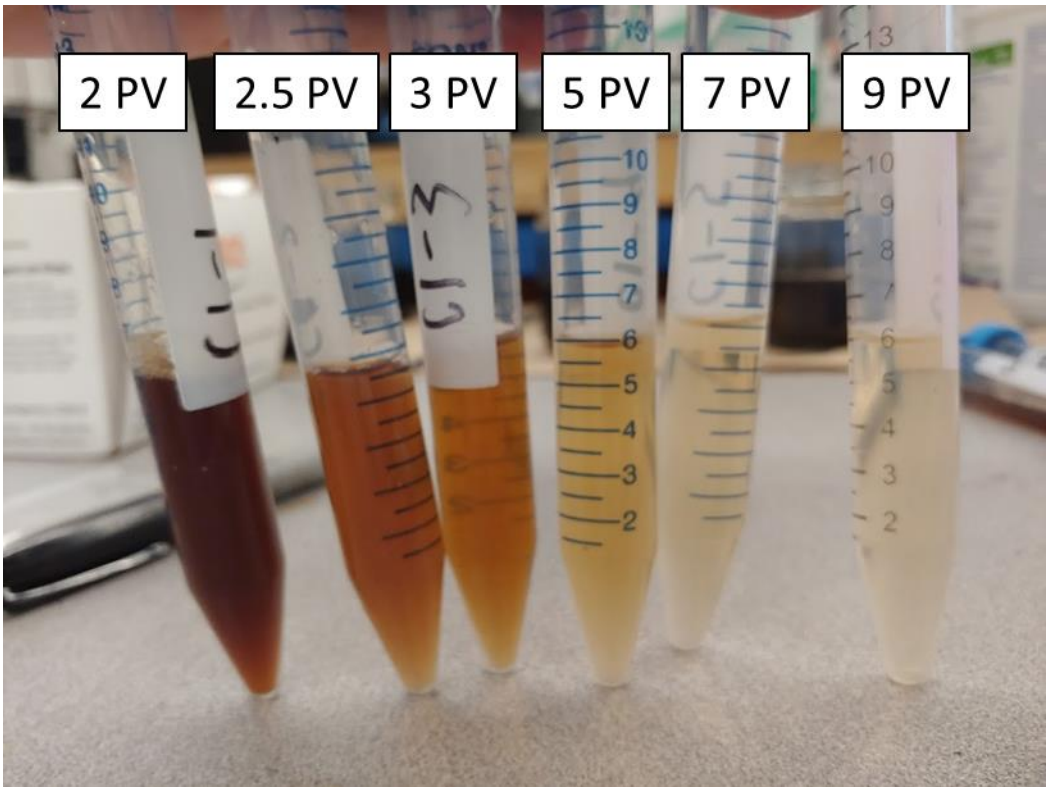

Figure 29: Colour change in leachate after adding 2, 2.5, 3, 5, 7, and 9 cumulative pore volumes (PV) of water

The cumulative releases of K and P in the collected leachate after adding 2, 2.5, 3, 5, 7, and 9 cumulative PV of DI water are shown in Figure 30 and Figure 31. The intervals between added PVs were small (0.5 PV) at the beginning as most of the K_3PO_4 was expected to leach out in this stage, after which the intervals increased to 2 PV. The fresh K_3PO_4 leached out of the columns quickly, with 60 and 70% of P and K released respectively after only 2 PV of water were added. 100% of each were released from the soil after 9 PVs of water were added. Compared to the fresh K_3PO_4, the coked K_3PO_4 remained in the soil column for longer time, suggesting that the coke does indeed provide a protective slow-release layer around the K_3PO_4 particles. Coke's ability to prevent leaching of both K and P varies with coking conditions: 1) 550 ^oC, 30 min, 2) 550 ^oC, 50 min, and 3) 350 ^oC, 30 min. The recycled coked K_3PO_4 (coked twice at 550 ^oC, 50 min) did not show a significant difference in leaching compared to the coked K_3PO_4 (coked only a single time) at the same condition (550 ^oC, 50 min). This suggests that recycling the spent catalyst does not noticeably improve the coking layer surrounding the K_3PO_4 particles.

The coke produced under 50 min had better K_3PO_4 retention than that produced under 30 min (3 and 8% decrease in K and P leaching, respectively), likely because the fraction of coke surrounding the K_3PO_4 particles is greater under 50 min of pyrolysis (as seen from TGA data in Figure 19). The coke produced at 350 °C had an even better K_3PO_4 retention (10 and 18% decrease in K and P leaching, respectively), likely because the oxygen functional groups remaining in the low temperature coke (see Figure 18) could create some electrostatic interactions with the K^+ and PO_4^- ions, especially the K^+ cations [77]. The release of PO_4^- could have been slowed by binding to cations within the soil, likely Mg^{2+}, Ca^{2+}, NH_4^+ and Na^+. Figure 32 depicts the suggested electrostatic interaction between K^+ ions and oxygen groups on coke produced at different temperatures.

This experiment proves that coke does indeed slow the release of K and P compared to the fresh K_3PO_4 in soil. However, to be considered a controlled-release fertilizer, the coating must release at least 15% of their nutrients by 24 h at room temperature, but no more than 75% after 28 days [61]. For agriculture use, the coked K_3PO_4 would remain mixed with the biochar before being added to soil. The biochar would improve both water retention and nutrient absorption, further decreasing the release of K and P into leachate. To test the efficacy in the future, biochar + coked K_3PO_4 samples should be mixed with soil and the release of K and P studied over several days of watering, mimicking the weather conditions of a specific region. Furthermore, for consideration as a controlled-release fertilizer, the release patterns must be predictable and will depend on soil conditions. This test should be repeated in soils of different composition and at different experimental temperatures to mimic greenhouse and/or outdoor growing conditions.

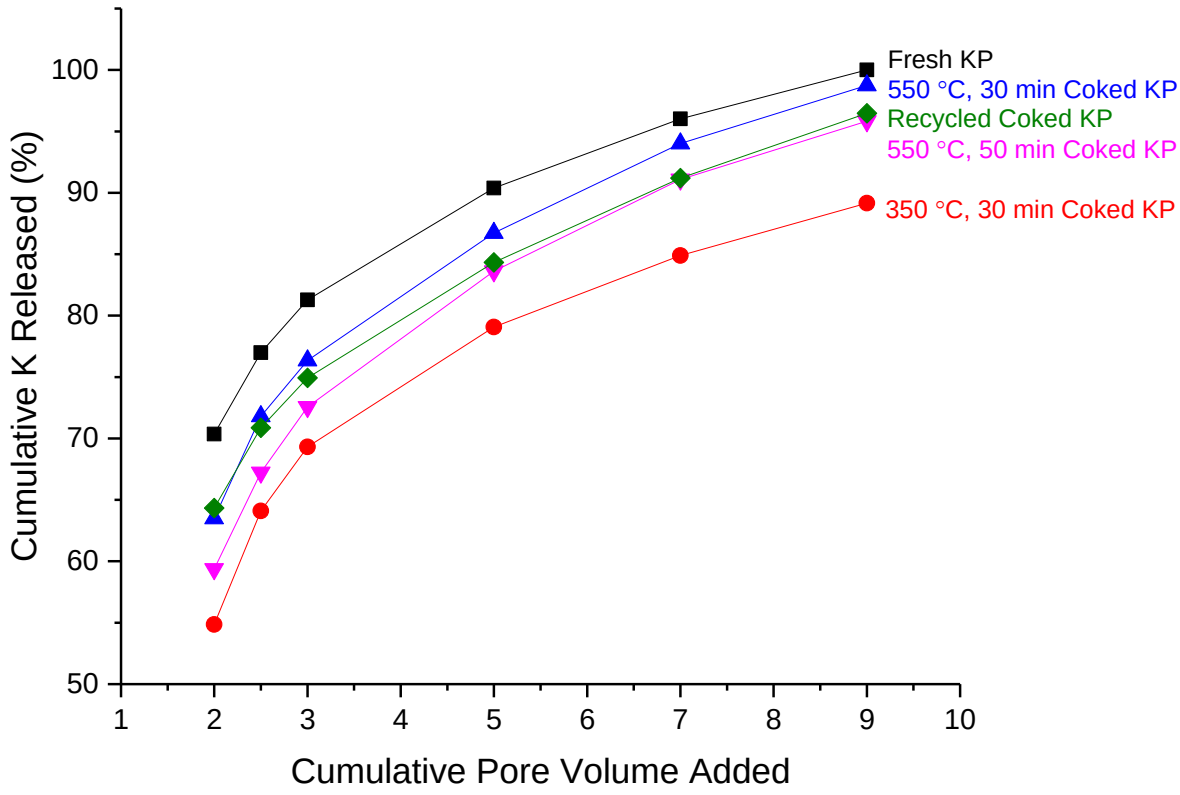

Figure 30: Cumulative release of K in the collected leachate of soil columns with different K_3PO_4 (KP) loadings

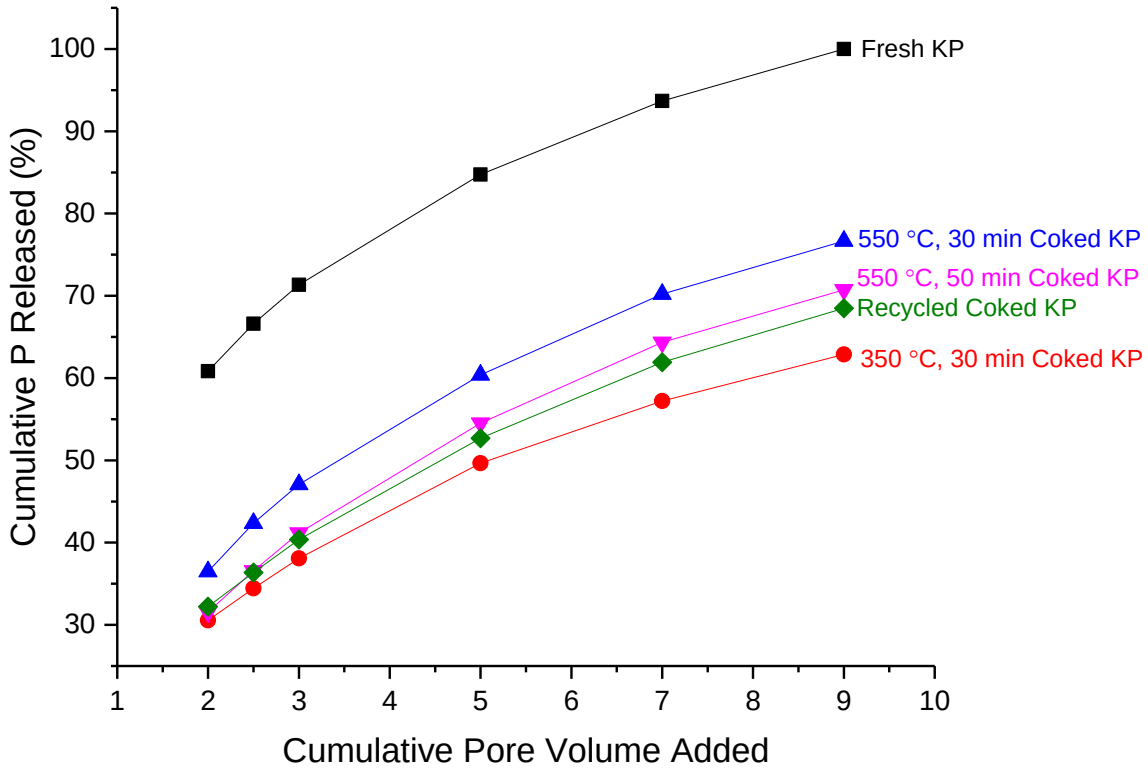

Figure 31: Cumulative release of P in the collected leachate of soil columns with different K_3PO_4 (KP) loadings

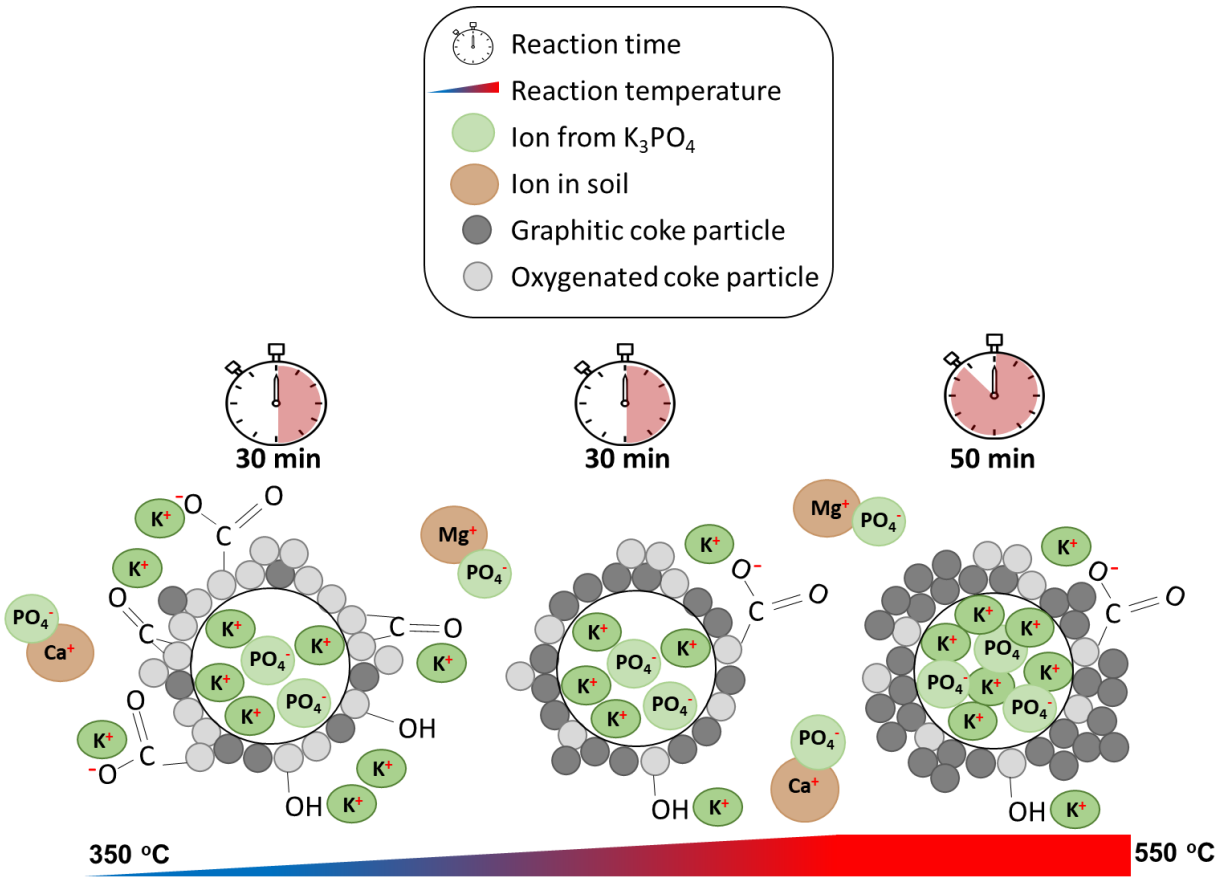

Figure 32: Suggested interactions between oxygen-containing functional groups and K^+ ions over coke produced at different temperatures. Adapted from [77].

4.4.1 Summary of Coke as a Slow-Release Fertilizer

Coke indeed slows the release of K and P into leachate from K_3PO_4 in soil. The slow release function is best in low-temperature coke; the coke produced at 350 °C for 30 min released 10 and 18 % less K and P, respectively, than the fresh K_3PO_4. The low temperature coke has more oxygen functional groups which can electrostatically interact with the leaching ions. The coke produced under a longer reaction time of 50 min also showed an improvement in K and P retention, likely because of the increased fraction of coke on the K_3PO_4 surface. It is estimated that coke produced at 350 °C for 50 min would have an even better retention in K and P as it has both advantages of a higher fraction of oxygen functional groups and a higher yield of coke.

Chapter 5: Conclusions and Future Work

This study attempted to offer input to two challenging questions: (1) how can we use wood waste as a resource to contribute to our circular economy, and (2) how can we prevent fertilizer emissions and leaching as crop demands increase? Pyrolysis of wood waste (sawdust) converts the feedstock into valuable biochar, which can be added to soils to decrease nutrient leaching and increase water retention. The use of microwaves during pyrolysis is found to heat sawdust more rapidly and more uniformly. However, with sawdust's low microwave absorption, a heat absorber and catalyst, K_3PO_4, is added to the feedstock. The K_3PO_4 acts also as a fertilizer downstream when added to soils alongside the produced biochar. During the pyrolysis reaction, a layer of coke forms on the surface of the K_3PO_4 particles. This study characterizes the coke and investigates its potential as a microwave absorber and as a slow-release barrier on the K_3PO_4 surface.

From DTG and EA analysis of the coke, it is revealed that increasing the coke preparation temperature between 350 – 550 °C increases the G:O ratio, suggesting that, at the higher reaction temperatures, the oxygen functional groups are cleaved off and the carbon structure becomes more polyaromatic. Data from TGA and EA also suggest that increasing the reaction time from 30 min to 50 min increases the yield of coke on the catalyst surface. The coke yield is greater at lower reaction temperatures. Both the increased G:O ratio and the increased coke yield lead to an increase in the coked K_3PO_4 microwave absorption. This is evident from both the measured loss tangent of the coked K_3PO_4 and the effect of recycling the coked K_3PO_4. The coke layer is also proved to be an effective slow-release barrier on the K_3PO_4 in soil. The slow release function is enhanced at

lower reaction temperatures (more oxygen-functional groups) and at longer reaction times (greater coke yield).

This study proves that the type and yield of coke that forms during pyrolysis can be tailored based on the reactor temperature and reaction time. It shows that graphitic coke does, indeed, absorb more microwaves than oxygenated coke, and thus can be recycled back into the reactor to improve the heating efficiency. The coke is also proven to be an effective slow release layer surrounding the K_3PO_4 particles. This layer can prevent groundwater contamination and soil acidification. In a scaled-up version of this study, the microwave reactor would likely operate as a fluidized bed to improve the heating uniformity between particles. During reaction, a portion of the biochar + coked K_3PO_4 mixture could be recycled back into the reactor to both improve the microwave absorption and increase the yield of coke on the K_3PO_4 particles. The product biochar + coked K_3PO_4 mixture would then be added to soil to gain benefits from both the biochar (water retention, improved soil structure, nutrient absorption) and from the coked K_3PO_4 (slow-release fertilizer). Before this process can be scaled-up though, some uncertainties and scale-up factors should be addressed:

1) The sawdust (300 – 600 μm) and K_3PO_4 (fine powder) feedstock is very heterogeneous when mixed, due to high variances in particle size. This leads to uncertainty in the reaction temperature, since the IR sensor measures only the top of the bed and may not be representative of the entire sample. This leads to variances between repeated runs.
2) Some uncertainties in analytical instrument should be addressed: Raman Spectroscopy of the coke did not show clear D and G peaks; the dielectric factors analyzer is meant to study solid and liquid samples (not powders), some variances occur then based on how the powder sample is pressed by the dielectric probe; the DTG data was analyzed using

peak analysis to generate a G:O ratio relationship, however, estimating a normal peak under the DTG curves does not accurately estimate the area under each curve.

3) Different feedstocks should be studied, such as wood waste (mixed woods, wood pellets, etc.) or food/municipal waste.
4) Finally, to make the process scale-up a viable option, some process parameters could be changed such as using recycled process vapours as the carrying gas and/or as an internal energy source for the system.
5) A life cycle assessment (LCA) should be carried out to determine the energy potentially saved by recycling the biochar and coke, and the potential economic benefits of using biochar + coked fertilizer vs. using the enhanced biochar + fresh fertilizer mixture in soils, among many other process factors.

References

[1] Ministry of Forests Mines and Lands, “The State of British Columbia’s Forests: Third Edition,” Victoria, 2010.

[2] H. Wang, “Environmental, economic and policy analysis of energy production from biomass residues in British Columbia,” University of British Columbia, 2019.

[3] Natural Resources Canada, “Mountain pine beetle (factsheet),” 2019. https://www.nrcan.gc.ca/forests/fire-insects-disturbances/top-insects/13397 (accessed Feb. 10, 2020).

[4] L. J. Corbett, P. Withey, V. A. Lantz, and T. O. Ochuodho, “The economic impact of the mountain pine beetle infestation in British Columbia: Provincial estimates from a CGE analysis,” *Forestry*, vol. 89, no. 1, pp. 100–105, Jan. 2016, doi: 10.1093/forestry/cpv042.

[5] Forest Enhancement Society of BC, “2020/21-2022/23 Service Plan,” Kamloops, 2020. Accessed: Mar. 11, 2020. [Online]. Available: https://fesbc.ca/.

[6] Sastistics Canada, “Analysis: Total Population,” 2018. https://www150.statcan.gc.ca/n1/pub/91-215-x/2018001/sec1-eng.htm (accessed Mar. 06, 2020).

[7] Agriculture and Agri-Food Canada, “CANADA: OUTLOOK FOR PRINCIPAL FIELD CROPS,” 2020.

[8] Statistics Canada, “Feeding the soil puts food on your plate,” 2015. https://www150.statcan.gc.ca/n1/pub/96-325-x/2014001/article/13006-eng.htm (accessed Mar. 06, 2020).

[9] M. Calabi-Floody *et al.*, *Smart Fertilizers as a Strategy for Sustainable Agriculture*, 1st ed., vol. 147. Elsevier Inc., 2018.

[10] P. M. Haygarth, R. D. Bardgett, and L. M. Condron, "Nitrogen and phosphorus cycles and their management," in *Soil Conditions and Plant Growth*, Oxford: Blackwell Publishing Ltd, 2013, pp. 132–159.

[11] Government of Manitoba, "Why Do Farmers Burn?" https://www.gov.mb.ca/agriculture/crops/crop-residue-burning-program/why-do-farmers-burn.html (accessed Mar. 06, 2020).

[12] J. J. Manyà, "Pyrolysis for biochar purposes: A review to establish current knowledge gaps and research needs," *Environmental Science and Technology*. 2012, doi: 10.1021/es301029g.

[13] D. Fytili and A. Zabaniotou, "Circular Economy Synergistic Opportunities of Decentralized Thermochemical Systems for Bioenergy and Biochar Production Fueled with Agro-industrial Wastes with Environmental Sustainability and Social Acceptance: a Review," *Curr. Sustain. Energy Reports*, vol. 5, no. 2, pp. 150–155, Jun. 2018, doi: 10.1007/s40518-018-0109-5.

[14] M. I. Jahirul, M. G. Rasul, A. A. Chowdhury, and N. Ashwath, "Biofuels production through biomass pyrolysis- A technological review," *Energies*, vol. 5, no. 12, pp. 4952–5001, 2012, doi: 10.3390/en5124952.

[15] D. Mohan, C. U. Pittman, and P. H. Steele, "Pyrolysis of wood/biomass for bio-oil: A critical review," *Energy and Fuels*, vol. 20, no. 3, pp. 848–889, 2006, doi: 10.1021/ef0502397.

[16] H. Yang, R. Yan, H. Chen, D. H. Lee, and C. Zheng, "Characteristics of hemicellulose,

cellulose and lignin pyrolysis," *Fuel*, vol. 86, no. 12–13, pp. 1781–1788, 2007, doi: 10.1016/j.fuel.2006.12.013.

[17] H. Bamdad, K. Hawboldt, and S. MacQuarrie, "A review on common adsorbents for acid gases removal: Focus on biochar," *Renewable and Sustainable Energy Reviews*, vol. 81. Elsevier Ltd, pp. 1705–1720, Jan. 01, 2018, doi: 10.1016/j.rser.2017.05.261.

[18] W. H. Chen, C. W. Wang, H. C. Ong, P. L. Show, and T. H. Hsieh, "Torrefaction, pyrolysis and two-stage thermodegradation of hemicellulose, cellulose and lignin," *Fuel*, vol. 258, Dec. 2019, doi: 10.1016/j.fuel.2019.116168.

[19] A. Skreiberg, O. Skreiberg, J. Sandquist, and L. Sørum, "TGA and macro-TGA characterisation of biomass fuels and fuel mixtures," *Fuel*, vol. 90, no. 6, pp. 2182–2197, Jun. 2011, doi: 10.1016/j.fuel.2011.02.012.

[20] P. Basu, *Biomass Gasification and Pyrolysis*. 2010.

[21] M. Gupta, J. Monnier, E. Turriff, and M. Boyd, "Partial deoxygenation of biomass derived pyrolysis liquids," *E3S Web Conf.*, vol. 61, 2018, doi: 10.1051/e3sconf/20186100018.

[22] D. Chiaramonti, A. Oasmaa, and Y. Solantausta, "Power generation using fast pyrolysis liquids from biomass," *Renewable and Sustainable Energy Reviews*. 2007, doi: 10.1016/j.rser.2005.07.008.

[23] S. E. Kolb, K. J. Fermanich, and M. E. Dornbush, "Effect of Charcoal Quantity on Microbial Biomass and Activity in Temperate Soils," *Soil Sci. Soc. Am. J.*, vol. 73, no. 4, pp. 1173–1181, Jul. 2009, doi: 10.2136/sssaj2008.0232.

[24] B. A. Mohamed, N. Ellis, C. S. Kim, and X. Bi, "The role of tailored biochar in increasing plant growth, and reducing bioavailability, phytotoxicity, and uptake of heavy metals in contaminated soil," *Environ. Pollut.*, vol. 230, pp. 329–338, Nov. 2017, doi:

10.1016/j.envpol.2017.06.075.

[25] L.-C. Sohi, “Biochar, climate change and soil: a review to guide future research,” 2009. doi: 10.4225/08/58597219A199A.

[26] I. Y. Eom *et al.*, “Effect of essential inorganic metals on primary thermal degradation of lignocellulosic biomass,” *Bioresour. Technol.*, vol. 104, pp. 687–694, 2012, doi: 10.1016/j.biortech.2011.10.035.

[27] A. Trendewicz, R. Evans, A. Dutta, R. Sykes, D. Carpenter, and R. Braun, “Evaluating the effect of potassium on cellulose pyrolysis reaction kinetics,” *Biomass and Bioenergy*, 2015, doi: 10.1016/j.biombioe.2015.01.001.

[28] Y. Le Brech *et al.*, “Effect of Potassium on the Mechanisms of Biomass Pyrolysis Studied using Complementary Analytical Techniques,” *ChemSusChem*, vol. 9, no. 8, pp. 863–872, Apr. 2016, doi: 10.1002/cssc.201501560.

[29] C. Di Blasi, C. Branca, and A. Galgano, “Influences of Potassium Hydroxyde on Rate and Thermicity of Wood Pyrolysis Reactions,” *Energy and Fuels*, vol. 31, no. 6, pp. 6154–6162, 2017, doi: 10.1021/acs.energyfuels.7b00536.

[30] D. J. Nowakowski, C. R. Woodbridge, and J. M. Jones, “Phosphorus catalysis in the pyrolysis behaviour of biomass,” *J. Anal. Appl. Pyrolysis*, vol. 83, no. 2, pp. 197–204, 2008, doi: 10.1016/j.jaap.2008.08.003.

[31] Q. Lu, Z. B. Zhang, X. C. Yang, C. Q. Dong, and X. F. Zhu, “Catalytic fast pyrolysis of biomass impregnated with K3PO 4 to produce phenolic compounds: Analytical Py-GC/MS study,” *J. Anal. Appl. Pyrolysis*, vol. 104, pp. 139–145, 2013, doi: 10.1016/j.jaap.2013.08.011.

[32] B. A. Mohamed, “Microwave-assisted catalytic pyrolysis of biomass for improving bio-oil

and biochar properties," The University of British Columbia, 2018.

[33] P. Chen *et al.*, "Utilization of municipal solid and liquid wastes for bioenergy and bioproducts production," *Bioresource Technology*, vol. 215. Elsevier Ltd, pp. 163–172, Sep. 01, 2016, doi: 10.1016/j.biortech.2016.02.094.

[34] Y. Zhang *et al.*, "Microwave-Assisted Pyrolysis of Biomass for Bio-Oil Production," in *Pyrolysis*, InTech, 2017.

[35] J. A. Menéndez *et al.*, "Microwave heating processes involving carbon materials," *Fuel Processing Technology*. 2010, doi: 10.1016/j.fuproc.2009.08.021.

[36] T. Kim, J. Lee, and K. H. Lee, "Full graphitization of amorphous carbon by microwave heating," *RSC Adv.*, vol. 6, no. 29, pp. 24667–24674, 2016, doi: 10.1039/c6ra01989g.

[37] D. Baird, E. Scerri, and L. McIntyre, *Production of Biofuels and Chemicals with Microwave*, vol. 3. 2015.

[38] C. Ellison, M. Sean McKeown, S. Trabelsi, and D. Boldor, "Dielectric Properties of Biomass/Biochar Mixtures at Microwave Frequencies," *Energies*, vol. 10, no. 4, pp. 502–514, 2017, doi: 10.3390/en10040502.

[39] J. A. Menéndez, A. Domínguez, Y. Fernández, and J. J. Pis, "Evidence of self-gasification during the microwave-induced pyrolysis of coffee hulls," *Energy and Fuels*, 2007, doi: 10.1021/ef060331i.

[40] B. A. Mohamed, N. Ellis, C. S. Kim, X. Bi, and A. E. R. Emam, "Engineered biochar from microwave-assisted catalytic pyrolysis of switchgrass for increasing water-holding capacity and fertility of sandy soil," *Sci. Total Environ.*, vol. 566–567, pp. 387–397, Oct. 2016, doi: 10.1016/j.scitotenv.2016.04.169.

[41] Y. Zhang, W. Zhao, B. Li, and G. Xie, "Microwave-Assisted Pyrolysis of Biomass for Bio-

Oil Production: A Review of the Operation Parameters," *J. Energy Resour. Technol.*, vol. 140, no. 4, 2018, doi: 10.1115/1.4039604.

[42] F. C. Borges *et al.*, "Fast microwave assisted pyrolysis of biomass using microwave absorbent," *Bioresour. Technol.*, vol. 156, pp. 267–274, Mar. 2014, doi: 10.1016/j.biortech.2014.01.038.

[43] A. Domínguez, J. A. Menéndez, M. Inguanzo, and J. J. Pís, "Production of bio-fuels by high temperature pyrolysis of sewage sludge using conventional and microwave heating," *Bioresour. Technol.*, vol. 97, no. 10, pp. 1185–1193, 2006, doi: 10.1016/j.biortech.2005.05.011.

[44] Y. Li *et al.*, "Coke formation on the surface of Ni/HZSM-5 and Ni-Cu/HZSM-5 catalysts during bio-oil hydrodeoxygenation," *Fuel*, vol. 189, pp. 23–31, 2017, doi: 10.1016/j.fuel.2016.10.047.

[45] M. Guisnet, L. Costa, and F. R. Ribeiro, "Prevention of zeolite deactivation by coking," *J. Mol. Catal. A Chem.*, vol. 305, no. 1–2, pp. 69–83, 2009, doi: 10.1016/j.molcata.2008.11.012.

[46] F. Li *et al.*, "Production of Light Olefins from Catalytic Cracking Bio-oil Model Compounds over La 2 O 3 -Modified ZSM-5 Zeolite," *Energy and Fuels*, vol. 32, no. 5, pp. 5910–5922, 2018, doi: 10.1021/acs.energyfuels.7b04150.

[47] Z. Xiong *et al.*, "Pyrolysis of the aromatic-poor and aromatic-rich fractions of bio-oil: Characterization of coke structure and elucidation of coke formation mechanism," *Appl. Energy*, vol. 239, no. January, pp. 981–990, 2019, doi: 10.1016/j.apenergy.2019.01.253.

[48] R. Sadeghbeigi, "Chemistry of FCC Reactions," *Fluid Catal. Crack. Handb.*, pp. 125–138, 2000, doi: 10.1016/b978-088415289-7/50005-6.

[49] B. Liu *et al.*, “Microwaves effectively examine the extent and type of coking over acid zeolite catalysts,” *Nat. Commun.*, vol. 8, no. 1, pp. 1–7, 2017, doi: 10.1038/s41467-017-00602-8.

[50] Y. Wei *et al.*, “Hydrocarbon produced from upgrading rich phenolic compound bio-oil with low catalyst coking,” *Fuel*, 2016, doi: 10.1016/j.fuel.2016.03.039.

[51] A. A. Al-Absi and S. S. Al-Khattaf, “Conversion of Arabian Light Crude Oil to Light Olefins via Catalytic and Thermal Cracking,” *Energy and Fuels*, vol. 32, no. 8, pp. 8705–8714, 2018, doi: 10.1021/acs.energyfuels.8b01932.

[52] M. Ternan, E. Furimsky, and B. I. Parsons, “Coke formation on hydrodesulphurization catalysts,” *Fuel Process. Technol.*, 1979, doi: 10.1016/0378-3820(79)90030-4.

[53] H. Zhang, S. Shao, R. Xiao, D. Shen, and J. Zeng, “Characterization of coke deposition in the catalytic fast pyrolysis of biomass derivates,” *Energy and Fuels*, vol. 28, no. 1, pp. 52–57, 2014, doi: 10.1021/ef401458y.

[54] D. Liu, L. Chen, L. Chen, R. Zheng, Q. Song, and G. Cai, “Influence of Conversion Conditions on Heavy-Oil Coking during in Situ Combustion Process,” *Energy and Fuels*, vol. 32, no. 4, pp. 4823–4832, 2018, doi: 10.1021/acs.energyfuels.8b00098.

[55] Z. Xiong *et al.*, “Evolution of coke structures during the pyrolysis of bio-oil at various temperatures and heating rates,” *J. Anal. Appl. Pyrolysis*, vol. 134, no. May, pp. 336–342, 2018, doi: 10.1016/j.jaap.2018.06.023.

[56] P. Pariyar, K. Kumari, M. K. Jain, and P. S. Jadhao, “Evaluation of change in biochar properties derived from different feedstock and pyrolysis temperature for environmental and agricultural application,” *Sci. Total Environ.*, vol. 713, Apr. 2020, doi: 10.1016/j.scitotenv.2019.136433.

[57] T. R. Carlson, G. A. Tompsett, W. C. Conner, and G. W. Huber, “Aromatic production from catalytic fast pyrolysis of biomass-derived feedstocks,” *Top. Catal.*, vol. 52, no. 3, pp. 241–252, 2009, doi: 10.1007/s11244-008-9160-6.

[58] F. Bauer and H. G. Karge, “Characterization of coke on zeolites,” *Mol. Sieves - Sci. Technol.*, 2006, doi: 10.1007/3829_005.

[59] M. Trenkel, *Improving Fertilizer Use Efficiency: Controlled-Release and Stabilized Fertilizers in Agriculture*. Paris: International Fertilizer Industry Association, 1997.

[60] T. Li, B. Gao, Z. Tong, Y. Yang, and Y. Li, “Chitosan and Graphene Oxide Nanocomposites as Coatings for Controlled-Release Fertilizer,” *Water. Air. Soil Pollut.*, vol. 230, no. 7, 2019, doi: 10.1007/s11270-019-4173-2.

[61] S. I. Sempeho, H. T. Kim, E. Mubofu, and A. Hilonga, “Meticulous Overview on the Controlled Release Fertilizers,” *Adv. Chem.*, vol. 2014, pp. 1–16, 2014, doi: 10.1155/2014/363071.

[62] K. Mikula *et al.*, “Controlled release micronutrient fertilizers for precision agriculture – A review,” *Sci. Total Environ.*, vol. 712, p. 136365, 2020, doi: 10.1016/j.scitotenv.2019.136365.

[63] B. Azeem, K. Kushaari, Z. B. Man, A. Basit, and T. H. Thanh, “Review on materials & methods to produce controlled release coated urea fertilizer,” *J. Control. Release*, vol. 181, no. 1, pp. 11–21, 2014, doi: 10.1016/j.jconrel.2014.02.020.

[64] M. Y. Naz and S. A. Sulaiman, “Slow release coating remedy for nitrogen loss from conventional urea: A review,” *Journal of Controlled Release*, vol. 225. Elsevier B.V., pp. 109–120, Mar. 10, 2016, doi: 10.1016/j.jconrel.2016.01.037.

[65] G. Hergert, R. Ferguson, C. Wortmann, C. Shapiro, and T. Shaver, “Enhanced Efficiency

Fertilizers: Will They Enhance My Fertilizer Efficiency?"

[66] M. Zhang, B. Gao, J. Chen, Y. Li, A. E. Creamer, and H. Chen, "Slow-release fertilizer encapsulated by graphene oxide films," *Chem. Eng. J.*, 2014, doi: 10.1016/j.cej.2014.06.023.

[67] Z. Ye, L. Zhang, Q. Huang, and Z. Tan, "Development of a carbon-based slow release fertilizer treated by bio-oil coating and study on its feedback effect on farmland application," *J. Clean. Prod.*, 2019, doi: 10.1016/j.jclepro.2019.118085.

[68] B. A. Mohamed, N. Ellis, C. S. Kim, and X. Bi, "Microwave-assisted catalytic biomass pyrolysis: Effects of catalyst mixtures," *Appl. Catal. B Environ.*, vol. 253, pp. 226–234, Sep. 2019, doi: 10.1016/j.apcatb.2019.04.058.

[69] H. A. Lutterding, "Soils the Langley-Vancouver Map Area Volume 6," Kelowna, 1981.

[70] Y. Liu, J. Tang, and Z. Mao, "Analysis of bread dielectric properties using mixture equations," *J. Food Eng.*, vol. 93, no. 1, pp. 72–79, Jul. 2009, doi: 10.1016/j.jfoodeng.2008.12.032.

[71] X. L. Bu, J. Su, J. H. Xue, Y. B. Wu, C. X. Zhao, and L. M. Wang, "Effect of rice husk biochar addition on nutrient leaching and microbial properties of Calcaric Cambisols," *J. Soil Water Conserv.*, vol. 74, no. 2, pp. 172–179, Mar. 2019, doi: 10.2489/jswc.74.2.172.

[72] A. J. Eykelbosh, M. S. Johnson, and E. G. Couto, "Biochar decreases dissolved organic carbon but not nitrate leaching in relation to vinasse application in a Brazilian sugarcane soil," *J. Environ. Manage.*, vol. 149, pp. 9–16, Feb. 2015, doi: 10.1016/j.jenvman.2014.09.033.

[73] S. Müller *et al.*, "Coke formation and deactivation pathways on H-ZSM-5 in the conversion of methanol to olefins," *J. Catal.*, vol. 325, pp. 48–59, 2015, doi:

10.1016/j.jcat.2015.02.013.

[74] G. van Rossum *et al.*, “Evaporation of pyrolysis oil: Product distribution and residue char analysis,” *AIChE J.*, vol. 56, no. 8, pp. 2211–2220, 2010, doi: 10.1002/aic.12126.

[75] F. Zikeli, V. Vinciguerra, A. R. Taddei, A. D’Annibale, M. Romagnoli, and G. S. Mugnozza, “Isolation and characterization of lignin from beech wood and chestnut sawdust for the preparation of lignin nanoparticles (LNPs) from wood industry side-streams,” *Holzforschung*, vol. 72, no. 11, pp. 961–972, 2018, doi: 10.1515/hf-2017-0208.

[76] X. Zhuang *et al.*, “Insights into the evolution of chemical structures in lignocellulose and non-lignocellulose biowastes during hydrothermal carbonization (HTC),” *Fuel*, vol. 236, no. September 2018, pp. 960–974, 2019, doi: 10.1016/j.fuel.2018.09.019.

[77] Y. Cai, H. Qi, Y. Liu, and X. He, “Sorption/Desorption Behavior and Mechanism of NH 4+ by Biochar as a Nitrogen Fertilizer Sustained-Release Material,” *J. Agric. Food Chem.*, vol. 64, no. 24, pp. 4958–4964, 2016, doi: 10.1021/acs.jafc.6b00109.

Appendix: ICP-OES Analysis

The total mass (m_{total} [mg]) of K and P per 1 g of coked K_3PO_4 was estimated using the ICP-OES results of K and P dissolved in the beaker of water:

$$m_{total} = \frac{C_{ICP} V_{ICP} V_{beaker}}{V_{collected}} = \frac{C_{ICP}(6\ mL)(50\ mL)}{1\ mL}$$

where C_{ICP} [mg/mL] is the concentration recorded from ICP-OES, V_{ICP} [mL] is the volume of liquid in the sample measured by ICP-OES, V_{beaker} [mL] is the volume of DI water initially added to the coked K_3PO_4, $V_{collected}$ [mL] is the volume of liquid collected from the beaker after 6 h.

The cumulative wt% of K and P released after each PV of DI water was calculated as:

$$\%released = \frac{m_{cumulative}}{m_{total}}$$

$$m_{cumulative} = \sum(m_{in\ each\ PV} - m_{in\ blank\ soil})$$

$$m_{in\ each\ PV} = \frac{C_{ICP} V_{ICP} V_{PV\ added}}{V_{collected}} = \frac{C_{ICP}(6\ mL)(V_{PV\ added})}{1\ mL}$$

where $m_{cumulative}$ [mg] is the cumulative mass of K and P leached after each PV of water was added, $m_{in\ each\ PV}$ [mg] is the individual mass of K and P leached after each set of PV's were added, $m_{in\ blank\ soil}$ is the mass of K and P released in the blank soil after each set of PV's were added, $V_{PV\ added}$ [mL] is the volume in each set of PV's.